

# Variational density functional calculations of excited states via direct optimization

Gianluca Levi,<sup>\*,†</sup> Aleksei V. Ivanov,<sup>†,‡</sup> and Hannes Jónsson<sup>†</sup>

<sup>†</sup>*Science Institute and Faculty of Physical Sciences, University of Iceland, 107 Reykjavík, Iceland*

<sup>‡</sup>*Saint Petersburg State University, 199034 Saint Petersburg, Russia.*

E-mail: giale@hi.is

## Abstract

The development of variational density functional theory approaches to excited electronic states is impeded by limitations of the commonly used self-consistent field (SCF) procedure. A method based on a direct optimization approach as well as the maximum overlap method is presented and the performance compared with previously proposed SCF strategies. Excited-state solutions correspond to saddle points of the energy as a function of the electronic degrees of freedom. The approach presented here makes use of a preconditioner determined with the help of the maximum overlap method to guide the convergence on a target  $n$ th-order saddle point. The method is found to be more robust and to converge faster than previously proposed SCF approaches for a set of 89 excited states of molecules. A limited-memory formulation of the symmetric rank-one method for updating the inverse Hessian is found to give the best performance. A conical intersection for the carbon monoxide molecule is calculated without resorting to fractional occupation numbers. Calculations on excited states of the hydrogen atom and a doubly excited state of the dihydrogen molecule using a self-interaction corrected functional are presented. For these systems, the self-interaction correction is found to

improve the accuracy of density functional calculations of excited states.

# 1 Introduction

In the light of recent and rapid advancements in fields such as photocatalysis and ultrafast spectroscopies, the availability of efficient and accurate computational methods to model electronic excited-state properties of molecules has become increasingly important. A widely used methodology to obtain excited-state properties of molecules is time-dependent density functional theory (TDDFT).<sup>1-3</sup> Practical applications of TDDFT rely on (i) linear response to describe the perturbation of the electron density due to an external field, and (ii) the adiabatic approximation, which neglects the time dependency of the functional derivative of the exchange-correlation (xc) potential with respect to the density, the so-called xc kernel. With those approximations, the computations can be carried out with local and semi-local ground-state Kohn-Sham (KS)<sup>4,5</sup> functionals without excessive computational requirements and this has been found to give an adequate description of valence excitations in many cases.<sup>1,6</sup> On the other hand, the neglect of the time dependency of the xc kernel limits the applicability of this approach and makes it, for example, inadequate for the description of double excitations<sup>7-9</sup> and conical intersections between ground and excited states.<sup>7,10</sup> Moreover, due to the incorrect form of the potential at long range and to the lack of orbital relaxation effects,<sup>11-13</sup> TDDFT with KS functionals suffers from systematic errors when applied to excited states that are diffuse, such as Rydberg states,<sup>6,14,15</sup> or involve transfer of charge between spatially separated regions.<sup>16-18</sup>

Some of these issues can be solved employing alternative DFT formulations where excited states are obtained as single Slater determinant wave functions optimized for non-aufbau occupations using ground-state functionals. Here, one seeks a saddle point on the energy surface instead of a minimum. Thanks to the inclusion of state-specific orbital relaxation

effects, these methods can describe a broader range of excited states than linear-response TDDFT in the adiabatic approximation, and have, therefore, seen a revival of interest recently.<sup>12,14,15,19–35</sup>

The excited-state DFT methodology that we consider here does not enforce orthogonality constraints between the different excited-state solutions and the ground state, and, therefore, represents a straightforward extension of ground-state DFT<sup>4</sup>. Higher-energy stationary points of ground-state density functionals obtained in this way do not necessarily represent rigorous approximations to the exact stationary states.<sup>15,36</sup> On the other hand, practice has shown that excited-state DFT calculations are usually able to deliver useful approximations to excited-state properties of molecules, such as excitation energies and potential energy surfaces.<sup>23,34</sup> Some studies have also highlighted how the method can satisfactorily treat cases, such as conical intersections, with strong static correlation, despite the single-determinant approximation<sup>19,22,22,33</sup>.

From a more practical point of view, the lack of orthogonality and the single-determinant approximation give rise to difficulties in the convergence of higher-energy solutions. First of all, when lower-energy states of the same symmetry are present, variational collapse can occur due to mixing of occupied and virtual orbitals with the same symmetry. The commonly used self-consistent field (SCF) approach can be combined with a maximum overlap method (MOM),<sup>15,23,34</sup> which prevents variational collapse. However, SCF convergence can still be problematic when dealing with single determinants that include unequally occupied degenerate or near-degenerate orbitals. This situation is analogous to what happens for ground states with vanishing HOMO-LUMO gap<sup>37</sup> and can arise, for example, close to conical intersections.<sup>38</sup> One strategy that is often adopted is electronic smearing to obtain convergence on an average occupied configuration.<sup>39</sup> This, however, comes with the risk of introducing artifacts in the calculated excited-state properties, as will be demonstrated below.

---

<sup>4</sup>Sometimes, this method is referred to as  $\Delta$  self-consistent field ( $\Delta$ SCF),<sup>21,24,28,32,33,35</sup> but here we prefer the more general term “excited-state DFT”, following Cheng *et al.*,<sup>15</sup> avoiding the risk of relating the method to a specific nonlinear variational procedure (such as SCF) and to the computation of a specific excited-state property (the excitation energy through the energy difference,  $\Delta$ , between excited and ground state).

There exist alternative nonlinear variational procedures for finding stationary points of energy functionals based on direct optimization (DO) of the orbitals through unitary transformations.<sup>40–43</sup> Implemented with gradient-based unconstrained optimization algorithms, this approach has been shown to be a more robust strategy for converging ground states with DFT than SCF-based methodologies.<sup>40,44,45</sup> However, the risk of variational collapse impedes straightforward application of DO methods for locating saddle points of the energy surface. One way of circumventing this problem is to convert the saddle-point optimization to a minimization of the squared norm of the gradient of the energy with respect to the electronic degrees of freedom.<sup>21</sup> Variational collapse is avoided by squared gradient minimization but there is a series of drawbacks that have to be considered. First, the computational cost is increased with respect to ground-state calculations, because the gradient of the squared norm of the gradient is needed. Furthermore, this strategy requires more iterations than SCF-MOM (when convergence can be reached),<sup>21</sup> because squared gradient minimization is less well conditioned than energy minimization.<sup>21,46</sup> Lastly, this approach can converge on points where the squared norm of the gradient has a minimum but is not zero. The initial guess, therefore, needs to be sufficiently good.<sup>21</sup>

When the above-mentioned practical issues have not represented a problem, excited-state calculations using KS functionals have given more accurate results than linear-response TDDFT for a number of challenging excited states. These include doubly excited states,<sup>21,23</sup> core excitations,<sup>20</sup> Rydberg<sup>15,21</sup> and charge-transfer<sup>23,26,34,47</sup> transitions, absorption spectra<sup>48</sup> and structural dynamics<sup>24,49</sup> in solution, including nonadiabatic dynamics<sup>19,22,33</sup>. However, it has been pointed out<sup>11,50</sup> that many excited states, such as Rydberg, charge-transfer and doubly excited states, are affected more by self-interaction error (SIE) than ground states at the level of the commonly employed semi-local KS functionals. An unbalanced treatment of self interaction can, for example, lead to systematic errors in calculations of excitation energy.<sup>11</sup> Self-interaction correction (SIC)<sup>51</sup> applied to KS functionals corrects the long-range form of the effective potential, as has been demonstrated, for example, for Rydberg states<sup>50</sup>

and dipole bound anions,<sup>52</sup> thus, it can improve the description of the excited states.<sup>53</sup> However, it is challenging to perform fully variational calculations with SIC functionals since they are explicitly orbital-density dependent and the energy is not invariant to unitary transformations among the equally occupied orbitals. While fully variational implementations of SIC functionals has been developed for ground states,<sup>54–57</sup> the excited-state calculations have so far not been fully variational.<sup>50</sup>

Here, we present a DO approach with the aim of improving on already existing excited-state DFT methodologies in two ways: (1) ensuring convergence for different types of excited states, including cases with unequally occupied degenerate orbitals, while avoiding variational collapse and without increasing the computational cost with respect to ground-state DFT calculations; (2) allowing the use of non-unitary invariant functionals, such as SIC functionals, in variational excited-state calculations. The proposed method uses a quasi-Newton algorithm to directly converge on saddle points of any order with the help of a preconditioner built from the eigenvalues of the Hamiltonian matrix at given intervals during the optimization, and MOM constraints to prevent variational collapse. A preliminary evaluation of the convergence properties of the DO-MOM method when using the Limited-memory Broyden-Fletcher-Goldfarb-Shanno (L-BFGS) algorithm and a new limited-memory formulation of Powell inverse Hessian update (L-Powell) is presented in a conference proceeding.<sup>58</sup> L-BFGS is a quasi-Newton method commonly employed for minimization, and it was shown that the application in the present context crucially depends on updates of the preconditioner and on the MOM constraints in order to converge on a saddle point. L-Powell was found to be less robust than L-BFGS,<sup>58</sup> despite its ability to generate indefinite Hessian approximations. It would be advantageous to attain convergence on a target  $n$ th-order saddle point without relying on updates of the preconditioner, since it requires costly diagonalization of the Hamiltonian matrix. In the present work, we extend the limited-memory inverse Hessian update algorithm presented in reference<sup>58</sup> to the symmetric rank-one (SR1) formula. SR1 can develop negative eigenvalues<sup>59</sup> and therefore has the desired characteristics to minimize

the dependency on the preconditioner.

The convergence properties of the DO-MOM method<sup>58</sup> are tested on 55 singlet and 34 triplet excited states of small and medium size molecules, including tests of the new limited-memory SR1 (L-SR1) inverse Hessian update algorithm. Furthermore, we test the convergence with respect to two challenging charge-transfer states of the nitrobenzene molecule, for which SCF-MOM has been reported to fail,<sup>21,60</sup> demonstrating that improved robustness and reduced dependency on the preconditioner can be achieved with the new L-SR1 method. Finally, we show how the DO-MOM method can converge for systems with unequally occupied (near-)degenerate orbitals without tuning modifications, taking the conical intersection of two excited states of carbon monoxide as a representative example. In each case, the performance of DO-MOM is compared to that of a standard SCF-MOM method.

The DO-MOM method can be used for non-unitary invariant functionals such as SIC functionals, as well as the unitary invariant KS functionals. We perform fully variational excited-state calculations with SIC on the hydrogen atom and dihydrogen molecule and show that the application of SIC in both ground- and excited-state calculations leads to significant improvement in the excitation energy.

## 2 Theory

### 2.1 Excited-State DFT

#### 2.1.1 Kohn-Sham Formulation

Within KS DFT,<sup>4,5</sup> excited states of a spin-polarized system of  $N = N_\uparrow + N_\downarrow$  electrons with density  $n(\mathbf{r}) = n_\uparrow(\mathbf{r}) + n_\downarrow(\mathbf{r})$  can be found as saddle points of the energy surface defined by the dependence of the ground-state energy on the electronic degrees of freedom:<sup>15</sup>

$$E_{\text{KS}}[n_\uparrow, n_\downarrow] = T_s[n_\uparrow, n_\downarrow] + V_{\text{ext}}[n] + J[n] + E_{\text{xc}}[n_\uparrow, n_\downarrow] \quad (1)$$

where  $T_s[n_\uparrow, n_\downarrow]$  is the kinetic energy of the non-interacting  $N$ -electron system,  $V_{\text{ext}}[n]$  and  $J[n]$  are the energy due to the external potential and the Hartree electrostatic energy, respectively:

$$V_{\text{ext}}[n] = \int \mathbf{v}_{\text{ext}}(\mathbf{r})n(\mathbf{r})d\mathbf{r} \quad (2)$$

$$J[n] = \frac{1}{2} \int \int \frac{n(\mathbf{r})n(\mathbf{r}')}{|\mathbf{r} - \mathbf{r}'|} d\mathbf{r}d\mathbf{r}' \quad (3)$$

while  $E_{\text{xc}}[n_\uparrow, n_\downarrow]$  is the exchange-correlation (xc) functional. The KS kinetic energy and the spin densities  $n_\sigma(\mathbf{r})$  are given in terms of orthonormal KS orbitals  $\psi_{n\sigma}(\mathbf{r})$ :

$$T_s[n_\uparrow, n_\downarrow] = -\frac{1}{2} \sum_{n\sigma} f_{n\sigma} \int \psi_{n\sigma}^*(\mathbf{r})\nabla^2\psi_{n\sigma}(\mathbf{r})d\mathbf{r} \quad (4)$$

$$n_\sigma(\mathbf{r}) = \sum_n f_{n\sigma} |\psi_{n\sigma}(\mathbf{r})|^2 \quad (5)$$

in which  $0 \leq f_{n\sigma} \leq 1$  is the occupation number for orbital  $n$  with  $\sigma$  spin quantum number ( $\uparrow$  or  $\downarrow$ ).

Stationary states of the non-interacting  $N$ -electron system can be obtained by finding extrema of the energy, eq. 1, subject to orbital orthonormality constraints:

$$\int \psi_{n\sigma}^*(\mathbf{r})\psi_{m\sigma'}(\mathbf{r})d\mathbf{r} = \delta_{nm}\delta_{\sigma\sigma'} \quad (6)$$

For a fixed set of  $f_{\sigma n}$ , the stationarity condition leads to a set of nonlinear coupled equations:

$$f_{n\sigma}\mathbf{H}_{\text{KS}}^\sigma\psi_{n\sigma} = \sum_m \lambda_{nm}^\sigma\psi_{m\sigma} \quad (7)$$

where the  $\lambda_{nm}^\sigma$  are Lagrange multipliers for the constraints, and  $\mathbf{H}_{\text{KS}}^\sigma$  is the one-particle KS

Hamiltonian:

$$\mathbf{H}_{\text{KS}}^\sigma = -\frac{1}{2}\nabla^2 + \mathbf{v}_{\text{ext}}(\mathbf{r}) + \int \frac{n(\mathbf{r}')}{|\mathbf{r} - \mathbf{r}'|} d\mathbf{r}' + \mathbf{v}_{\text{xc}}^\sigma(\mathbf{r}) \quad (8)$$

For a functional with a form given by eq. 1, any unitary transformation that mixes equally occupied orbitals among themselves leaves the total energy unchanged. Therefore, the set of orbitals that makes the energy stationary for given set of occupation numbers is not unique.

### 2.1.2 Self-Interaction Correction

In KS functionals, the Coulomb interaction between the electrons is estimated from the total electron density, and hence it includes non-local self interaction. While the xc functional also includes self interaction of opposite sign, a local or semi-local functional form cannot cancel out the self Coulomb interaction and a SIE remains, as can be seen most clearly for one-electron systems. Perdew and Zunger<sup>51</sup> proposed the following procedure for removing self interaction from a KS functional:

$$E_{\text{SIC}}[n_\uparrow, n_\downarrow] = E_{\text{KS}}[n_\uparrow, n_\downarrow] - \sum_{n\sigma} (J[n_{n\sigma}] + E_{\text{xc}}[n_{n\sigma}, 0]) \quad (9)$$

where  $n_{n\sigma} = |\psi_{n\sigma}|^2$  is an orbital density. This represents an orbital-by-orbital estimate of the SIE that is exact for one-electron systems.

For a SIC functional, the stationarity condition leads to a set of nonlinear coupled equations:

$$f_{n\sigma} (\mathbf{H}_{\text{KS}}^\sigma - \mathbf{V}_{n\sigma}) \psi_{n\sigma} = \sum_m \lambda_{nm}^\sigma \psi_{m\sigma} \quad (10)$$

where the Hamiltonian contains an orbital-density dependent part:

$$\mathbf{V}_{n\sigma} = \int \frac{n_{n\sigma}(\mathbf{r}')}{|\mathbf{r} - \mathbf{r}'|} d\mathbf{r}' + \mathbf{v}_{\text{xc}}(n_{n\sigma}) \quad (11)$$

In contrast to KS functionals, SIC functionals are not invariant under unitary transformations of the equally occupied orbitals, and the optimal orbitals are uniquely defined as those that extremize the energy of the given SIC functional.<sup>54–57,61–63</sup> This corresponds to maximizing the self-interaction correction, and involves unitary optimization within the manifold of occupied orbitals.

## 2.2 Self-Consistent Field

For unitary invariant functionals, eq. 7 can be simplified by choosing a unitary transformation that diagonalizes  $\lambda^\sigma$  while leaving the energy unchanged, leading to the generalized KS eigenvalue equations in the canonical form:

$$\mathbf{H}_{\text{KS}}^\sigma \psi_{n\sigma}(\mathbf{r}) = \epsilon_{n\sigma} \psi_{n\sigma}(\mathbf{r}) \tag{12}$$

For the non-unitary invariant SIC functionals presented in the previous section, the Lagrange matrix is not diagonal for the optimal orbitals that extremize the total SIC-DFT energy due to the orbital-density dependence.<sup>56,61,64</sup>

Solutions to the KS equations are found iteratively, defining the SCF procedure. The ground state corresponds to a minimum of the energy given by the functional and is obtained if at each SCF iteration the orbitals are occupied according to the aufbau principle. Saddle points on the energy surface are obtained for non-aufbau occupations and are interpreted as excited states.<sup>15,21,65</sup> Non-aufbau occupations can be enforced during the SCF cycle through the MOM method: at each iteration, the occupied orbitals are selected as those that overlap most with the occupied orbitals of the previous iteration<sup>34</sup> or with a set of fixed reference orbitals<sup>15,23</sup> (the latter strategy is also known as initial maximum overlap method (IMOM)<sup>23</sup>).

## 2.3 Direct Optimization

Alternatively, the variational problem can be formulated as an optimization of the orbitals through application of a unitary transformation to a set of orthonormal reference orbitals:<sup>40–43</sup>

$$\phi_{p\sigma}(\mathbf{r}) = \sum_q U_{pq}^\sigma \psi_{q\sigma}(\mathbf{r}) \quad (13)$$

The unitary matrix  $\mathbf{U}$  can be parametrized as the matrix exponential:<sup>41,42</sup>

$$\mathbf{U} = e^\theta \quad (14)$$

where  $\theta$  is required to be anti-Hermitian ( $\theta = -\theta^\dagger$ ) in order to preserve the orbital orthonormality. In this way, the energy functional can be directly extremized in the linear space formed by anti-Hermitian matrices, which makes it possible to use well-established local unconstrained optimization strategies.<sup>59</sup> The exponential transformation of molecular orbitals can be applied to both KS and SIC functionals, since it does not require the functional to be unitary invariant (unitary optimization for SIC functionals means that the elements of  $\theta$  that mix occupied orbitals are non-zero in contrast to KS functionals, as explained in the next section). Moreover, gradient-based direct optimization (DO) ensures more rigorous convergence compared to SCF.<sup>40,65</sup>

For excited states, the unconstrained search can be done with quasi-Newton methods that are able to locate saddle points. Compared to minimization, the search for a saddle point is arguably a more challenging task, requiring an initial guess that is sufficiently close to the wanted solution and a good approximation to the Hessian. Nevertheless, quasi-Newton methods for saddle points have long been employed with some success in various contexts, most notably transition-state searches on potential energy surfaces for atomic rearrangements.<sup>66–71</sup> Here, we explore a strategy for DO of saddle points of KS and SIC density

functionals using quasi-Newton search directions starting from a guess obtained by promoting one or more electrons from occupied to unoccupied orbitals of a converged ground-state calculation.

### 3 Implementation

We have implemented DO-MOM with KS and SIC functionals in a development branch of the Grid-based Projector Augmented Wave (GPAW)<sup>72-74</sup> software using localized atomic basis sets to represent the molecular orbitals. The implementation of the exponential transformation for KS functionals is presented in Reference.<sup>58</sup> A review of this implementation and its extension to SIC functionals are given in Appendix A. The MOM is based on a standard implementation using fixed reference orbitals<sup>23</sup> as shown in Appendix C. In the following, we describe the new L-SR1 algorithm, including the choice of preconditioner.

#### 3.1 Quasi-Newton Step

The computational effort of a quasi-Newton step based on updating the Hessian matrix scales as  $\mathcal{O}(n^3)$ ,<sup>59</sup> where  $n$  is the dimensionality of the optimization problem (the present DO implementation based on exponential transformation scales as  $NM$ , where  $N$  is the number of occupied orbitals and  $M$  the number of basis set functions). A less computationally demanding approach is to update the inverse Hessian instead of the Hessian, since this does not involve any matrix-matrix operation or solution of a linear system of equations. The quasi-Newton step with inverse Hessian update is:

$$\mathbf{x}^{(k+1)} = \mathbf{x}^{(k)} - \mathbf{B}^{(k)} \mathbf{g}^{(k)} \tag{15}$$

where  $\mathbf{B}^{(k)}$  is the approximate inverse Hessian at iteration  $k$ , and  $\mathbf{x}^{(k)}$  and  $\mathbf{g}^{(k)}$  are the vectors of the  $\{\theta_{ij}\}$  independent variables and the analytical gradient, respectively.

When the inverse Hessian is updated, the arithmetic operations scale as  $\mathcal{O}(n^2)$ ,<sup>59</sup> which

can become a bottleneck for systems with a moderate number of electrons and/or large basis sets. To circumvent the costly operations embedded in the explicit update and storage of the Hessian matrix, quasi-Newton algorithms can be formulated in a limited-memory version by storing only vectors and scalars carrying the information necessary to propagate  $\mathbf{B}$  implicitly. In this case, the operations involved in one iteration scale linearly as  $\mathcal{O}(mn)$ , where  $m$  is the number of previous steps used to update the current step.

L-BFGS is a commonly used limited-memory version of BFGS, which is generally considered to be the most effective inverse Hessian update for minimization. The L-BFGS method has been implemented here as described in reference.<sup>59</sup> In calculations of atomic structures, the Powell or SR1 Hessian update formulas, or a combination of the two,<sup>67,75</sup> are preferred for saddle-point searches, because they are able to develop negative eigenvalues contrary to the BFGS formula. Therefore, we have formulated and implemented limited-memory variants of the Powell and SR1 inverse Hessian updates (L-Powell and L-SR1) by extending the approach based on Powell Hessian updates presented by Anglada *et al.*<sup>76</sup> The L-Powell method is described in reference<sup>58</sup> and is reviewed in Appendix B.

The inverse Hessian SR1 update formula, written in a compact form, is:<sup>77</sup>

$$\mathbf{B}_{\text{SR1}}^{(k+1)} = \mathbf{B}^{(k)} + \frac{\mathbf{j}^{(k)}\mathbf{j}^{T(k)}}{\mathbf{j}^{T(k)}\mathbf{y}^{(k)}} \quad (16)$$

where:

$$\mathbf{j}^{(k)} = \mathbf{s}^{(k)} - \mathbf{B}^{(k)}\mathbf{y}^{(k)}, \quad (17)$$

and:

$$\mathbf{s}^{(k)} = \mathbf{x}^{(k+1)} - \mathbf{x}^{(k)}, \quad \mathbf{y}^{(k)} = \mathbf{g}^{(k+1)} - \mathbf{g}^{(k)} \quad (18)$$

For any vector  $\mathbf{v}^{(k)}$  and approximation  $\mathbf{B}_0^{(k)}$  to the inverse Hessian ( $\mathbf{B}_0^{(k)}$  can in principle be

allowed to vary at each iteration),  $\mathbf{B}_{\text{SR1}}^{(k)} \mathbf{v}^{(k)}$  can be computed using the following recursive formula:

$$\mathbf{B}_{\text{SR1}}^{(k)} \mathbf{v}^{(k)} = \mathbf{B}_0^{(k)} \mathbf{v}^{(k)} + \sum_{i=k-m}^{k-1} \frac{\mathbf{j}^{(i)} \mathbf{j}^{T(i)} \mathbf{v}^{(k)}}{\mathbf{j}^{T(i)} \mathbf{y}^{(i)}} \quad (19)$$

which takes into account the implicit information contained in the  $m$  most recent steps.

Using this result, the L-SR1 algorithm can be formulated as shown in Algorithm 1.

```

Choose  $\mathbf{x}^{(0)}$ ,  $m$  and  $p_{\max}$ ;
 $k \leftarrow 0$ ;
while not converged do
  Choose  $\mathbf{B}_0^{(k)}$ ;
  Compute  $\mathbf{p}^{(k)} \leftarrow \mathbf{B}^{(k)} \mathbf{g}^{(k)}$  using eq. 19;
  if  $\|\mathbf{p}^{(k)}\| \geq p_{\max}$  then
     $\mathbf{p}^{(k)} \leftarrow \frac{p_{\max}}{\|\mathbf{p}^{(k)}\|} \mathbf{p}^{(k)}$ 
  end
   $\mathbf{x}^{(k+1)} \leftarrow \mathbf{x}^{(k)} - \mathbf{p}^{(k)}$ ;
  if  $k > m$  then
    discard vector  $\mathbf{j}^{(k-m)}$  and scalar  $r^{(k-m)}$ ;
  end
   $\mathbf{s}^{(k)} \leftarrow \mathbf{x}^{(k+1)} - \mathbf{x}^{(k)}$  and  $\mathbf{y}^{(k)} \leftarrow \mathbf{g}^{(k+1)} - \mathbf{g}^{(k)}$ ;
  Compute  $\mathbf{j}^{(k)} \leftarrow \mathbf{B}^{(k)} \mathbf{y}^{(k)}$  using eq. 19;
   $\mathbf{j}^{(k)} \leftarrow \mathbf{s}^{(k)} - \mathbf{j}^{(k)}$ ;
   $r^{(k)} \leftarrow \mathbf{j}^{T(k)} \mathbf{y}^{(k)}$ ;
  Store vector  $\mathbf{j}^{(k)}$  and scalar  $r^{(k)}$ ;
   $k \leftarrow k + 1$ ;
end

```

**Algorithm 1:** Quasi-Newton algorithm with limited-memory SR1 inverse Hessian update. The computational cost of the operations involved scales linearly with  $n$  if  $\mathbf{B}_0^{(k)}$  is selected to be diagonal.

Among the quasi-Newton schemes that are commonly used in optimizations of saddle points for atomic rearrangements, some update the Hessian through a combination of the SR1 and Powell updates. Algorithm 1 is readily generalized to use an analogous update

formula that combines the SR1 and Powell inverse Hessian updates:

$$\mathbf{B}_\phi^{(k+1)} = (1 - \phi^k)\mathbf{B}_{\text{SR1}}^{(k+1)} + \phi^k\mathbf{B}_{\text{P}}^{(k+1)} \quad (20)$$

where  $\mathbf{B}_{\text{SR1}}^{(k+1)}$  and  $\mathbf{B}_{\text{P}}^{(k+1)}$  are given by eqs. 16 and B.1, respectively. Following Bofill,<sup>67,75</sup> the factor  $\phi^k$  can be taken as:

$$\phi^k = 1 - \frac{(\mathbf{y}^{T(k)}\mathbf{j}^{(k)})^2}{(\mathbf{y}^{T(k)}\mathbf{y}^{(k)})(\mathbf{j}^{T(k)}\mathbf{j}^{(k)})} \quad (21)$$

In Algorithm 1 we have also introduced a maximum allowed step length,  $p_{\text{max}}$ . This is because, due to the approximate nature of the initial approximation to the Hessian (see next section), initial steps may be too large, causing departure from the basin of attraction of the desired saddle point. We have found that  $p_{\text{max}} = 0.20$  provides an adequate balance between stability and speed of convergence in most cases. The SR1 update can become unstable if the denominator in eq. 16 is small. To avoid such instabilities, the following procedure is adopted: if  $|\mathbf{j}^{T(i)}\mathbf{y}^{(i)}| < \varepsilon$ , where  $\varepsilon$  is a small number, then  $\mathbf{j}^{T(i)}\mathbf{y}^{(i)}$  is set to  $\varepsilon$ . When using  $\varepsilon = 10^{-12}$ , we have found that this procedure prevents L-SR1 from becoming unstable, without affecting the rate of convergence.

### 3.2 Preconditioner

The preconditioner for the quasi-Newton step, represented by the matrix  $\mathbf{B}_0^{(k)}$  introduced in the previous section, is chosen as the inverse of the following diagonal approximation to the Hessian matrix:<sup>42</sup>

$$\frac{\partial^2 E}{\partial^2 \theta_{ij}} \approx -2(\epsilon_i - \epsilon_j)(f_i - f_j) \quad (22)$$

where the  $\epsilon_i$  are the eigenvalues of the Hamiltonian matrix. Eq. 22 is obtained by taking the derivative of a linear expansion of the gradient (eq. A.6) and neglecting second-order

derivatives of the potential. Previously, it has been shown that this type of preconditioner can improve the convergence of Hartree-Fock (HF) and DFT calculations based on direct minimization of the energy,<sup>21,40</sup> when using the BFGS method.

At the beginning of the optimization, the preconditioner is generated using the eigenvalues and occupation numbers of the guess obtained by promoting electrons from occupied to virtual orbitals of the ground state. As will be shown for the excited states of nitrobenzene, it can happen that the number of negative eigenvalues of this initial approximate Hessian is not consistent with the order of the saddle point corresponding to the target excited state. To ensure that the preconditioner has the appropriate structure to guide the convergence towards the target  $n$ th-order saddle point, the approximate Hessian of eq. 22 is recomputed at regular intervals during the optimization and  $\mathbf{B}_0^{(k)}$  updated together with the reference orbitals. In order to find the occupation numbers of the canonical orbitals, which are needed to compute the preconditioner based on eq. 22, the MOM method is employed (see Appendix C). Close to the target solution, the update of the preconditioner is not needed and can be avoided using a threshold on the magnitude of the energy gradient, which reduces the computational cost by avoiding unnecessary diagonalization of the Hamiltonian matrix. Finally, we note that the preconditioner derived from eq. 22 is not defined for oo terms, since in this case  $f_i^{(k)} = f_j^{(k)}$ , and for degenerate ov pairs. For these cases, the preconditioner is not used, corresponding to setting the elements of  $\mathbf{B}_0^{(k)}$  to 1.

## 4 Computational Methods

All the calculations presented in this work are performed with a development version of GPAW where the DO-MOM method for KS and SIC xc functionals has been implemented. The PAW method<sup>78</sup> is used to treat the regions near the nuclei, core electrons of each atom are frozen to the result of a reference scalar relativistic calculation of the isolated atom, and valence electrons are represented in a basis of linear combination of atomic orbitals. For

all the basis sets considered in this work, the uncontracted functions are removed, as the nodal structure of the orbitals around the nuclei is accounted for by the PAW correction. The simulation cell has a uniform grid with grid spacing of 0.15 Å, while the dimensions of the box are chosen in such a way as to avoid effects due to truncation of the numerical representation of the basis functions. For the DO-MOM calculations, a maximum allowed step length,  $p_{\max}$ , of 0.20 is utilized, while the memory  $m$  of L-BFGS, L-Powell and L-SR1 is chosen as equal to 20. At every 20th step the preconditioner based on eq. 22 is updated unless the root mean square of the gradient is less than  $10^{-3}$  eV. The SCF-MOM method is based on direct diagonalization of the Hamiltonian matrix in the basis of atomic orbitals and updating the electron density using a direct inversion in the iterative subspace (DIIS) procedure (Pulay mixing of the density<sup>72,79</sup>). We use GPAW default parameters for the Pulay mixing of the density: the number of old densities used in the mixing is 3, the coefficient used in the linear mixing of the density with the density residual vector is 0.15, and no damping of short wavelength density changes is used.<sup>72</sup> Unless otherwise stated, convergence (both in SCF or DO calculations) is considered achieved if the integrated value of the square of the residuals of eq. 7 (for KS functionals) or 10 (for SIC functionals) is less than  $4.0 \cdot 10^{-8}$  eV<sup>2</sup> per electron. All calculations are performed within the spin-unrestricted formalism. Since each state is described by a single determinant, open-shell singlets are not pure-spin states. Both the KS and SIC calculations use the generalized gradient approximation (GGA) functional PBE.<sup>80</sup>

## 4.1 Convergence Tests

The robustness and rate of convergence of the DO-MOM method is assessed by performing single-point calculations of the excited states of small and medium size molecules. The tests include 52 singlet and 34 triplet excited states of 18 small compounds from the benchmark set of reference,<sup>81</sup> and the lowest singlet excited states of 3 medium organic compounds (acetone, benzene and naphthalene) from reference,<sup>82</sup> for a total of 89 states generated by

single electron transition from the ground state. Lowest triplet states have been excluded from this benchmark set since they correspond to minima on the energy surface and not saddle points. These states are chosen because highly accurate reference data is available making reliable assignment of the states possible, and due to the diverse character of the electronic transitions. The test set includes 35 valence (V) excitations ( $n \rightarrow \pi^*$ ,  $\sigma \rightarrow \pi^*$  and  $\pi \rightarrow \pi^*$  transitions), 53 Rydberg (R), and 1 charge-transfer (CT) states (the lowest singlet excited state of hydrogen chloride). The geometries are taken from reference<sup>81</sup> and reference.<sup>82</sup> For the DO-MOM calculations three different inverse Hessian update schemes are compared: L-BFGS, L-Powell and L-SR1 (the latter two according to the limited-memory algorithm presented in section 3.1). We further compare DO-MOM to a standard SCF-MOM method based on direct diagonalization of the Hamiltonian matrix, as implemented in GPAW.<sup>73</sup> For each molecule, the ground state is first converged using SCF. Then, the initial guess for an excited state is generated by a one-electron excitation involving the occupied and unoccupied orbitals that define the character and symmetry of the excited state. Convergence is obtained when the square of the residuals is less than  $10^{-10}\text{eV}^2$ . The maximum number of iterations for a calculation is 300. The *aug-cc-pVDZ* basis set<sup>83-85</sup> is used.

The calculations of nitrobenzene test both SCF-MOM and DO-MOM with L-BFGS and L-SR1 with respect to convergence to the singlet  ${}^1A_1(n_\pi \rightarrow \pi^*)$  and  ${}^1A_1(\pi' \rightarrow \pi^*)$  excited states. Using the ground-state orbitals, the initial guess for the  ${}^1A_1(n_\pi \rightarrow \pi^*)$  state is generated by promoting an electron from the highest energy  $\pi$  lone pair ( $n_\pi$ ) to the second lowest  $\pi^*$  orbital ( $\pi'^*$ ), while for the  ${}^1A_1(\pi' \rightarrow \pi^*)$  state excitation is from the second highest occupied  $\pi$  orbital ( $\pi'$ ) to the lowest unoccupied  $\pi^*$  orbital. The calculations are performed at the  $C_{2v}$  geometry used in references.<sup>21,60</sup> The basis set is def2-TZVP,<sup>86</sup> as in the calculations presented in references.<sup>21,60</sup>

To further assess the robustness of the DO-MOM method in cases of orbital degeneracy, the potential energy curves (PECs) of the lowest  ${}^1\Pi(\sigma \rightarrow \pi^*)$  and  ${}^1\Delta(\pi \rightarrow \pi^*)$  excited states

of carbon monoxide are calculated around the conical intersection. The DO-MOM PECs and analytical atomic forces are compared with PECs and forces obtained using an SCF-MOM method where convergence is attained through Gaussian smearing of both the hole and the excited electron.<sup>24</sup> Let  $N$  denote the number of valence electrons described explicitly and  $M$  the total number of orbitals included in the calculation. At each SCF step, the hole  $i$  and the excited orbital  $a$  are determined through the maximum overlap criterion and the occupation numbers of the  $n$  lowest  $N$  orbitals and those of the  $m$  orbitals from  $N + 1$  to  $M$  are modified according to:

$$f_n(\epsilon_n) = 1 - s_i(\epsilon_n) \tag{23}$$

$$f_m(\epsilon_m) = s_a(\epsilon_m) \tag{24}$$

where  $s_i(\epsilon_n)$  and  $s_a(\epsilon_m)$  are Gaussian functions of the KS eigenvalues:

$$s_i(\epsilon_n) = \frac{1}{A_i} \exp \left[ -\frac{(\epsilon_n - \epsilon_i)^2}{2\sigma^2} \right], \quad s_a(\epsilon_m) = \frac{1}{A_a} \exp \left[ -\frac{(\epsilon_m - \epsilon_a)^2}{2\sigma^2} \right] \tag{25}$$

with the normalization factors being such that the total number of electrons is conserved. The width  $\sigma$  is chosen as 0.01 eV at the beginning of the SCF and then it is increased by 0.02 eV every 40th iterations, until convergence is reached. A similar electronic smearing technique has been used before to stabilize the SCF convergence in DFT calculations of PECs<sup>33</sup> and Born-Oppenheimer molecular dynamics simulations with DFT atomic forces.<sup>24,49,87</sup> For all the calculated points of both DO-MOM and SCF-MOM PECs, the guess orbitals are from a ground-state calculation at the reference geometry,<sup>81</sup> where the interatomic distance is 1.134 Å. The DO-MOM and SCF-MOM calculations of the PECs of carbon monoxide use a dzp basis<sup>73</sup> (default in GPAW).

## 4.2 Self-Interaction Corrected Calculations

DO-MOM calculations were carried out of the ground and first three lowest excited states of the hydrogen atom and of the ground and  $^1\Sigma_g^+(1\sigma_g^2 \rightarrow 1\sigma_u^2)$  doubly excited state of the dihydrogen molecule using both PBE and SIC-PBE. The basis sets are *daug*-cc-pV6Z excluding *g*- and *h*-type functions for hydrogen, and *aug*-mcc-pVQZ excluding *f*-type functions for dihydrogen, which leads to an excitation energy converged to within  $\sim 0.01$  eV (see Figure S1 in the Supporting Information) The interatomic distance in dihydrogen is set to 1.4 Å as in reference.<sup>23</sup>

# 5 Results

## 5.1 Convergence Tests

### 5.1.1 Benchmarks on Small and Medium Size Molecules

The results of the convergence tests on 55 singlet and 34 triplet excited states of small and medium size molecules are reported in Tables 1 and 2. The average, maximum and

Table 1: Convergence properties of the SCF-MOM and DO-MOM methods for 52 singlet excited states of molecules from the benchmark set in reference<sup>81</sup> plus the lowest excited states of acetone, benzene and naphtalene. For the DO-MOM methods, one iteration corresponds to one energy and gradient evaluation, while for SCF-MOM it represents one energy evaluation and finding the solution for the eigendecomposition of the Hamiltonian matrix.

	SCF-MOM	DO-MOM		
		L-BFGS	L-Powell	L-SR1
Convergence failures	17	2	10	0
Avg no. iterations	22.9	13.9	20.5	12.3
Max no. iterations	96	32	69	17
Min no. iterations	15	9	9	9
Local saddle points	0	1	1	1

minimum number of iterations are reported after excluding the cases that do not converge

Table 2: Convergence properties of the SCF-MOM and DO-MOM methods for 34 triplet states of molecules from the benchmark set in reference.<sup>81</sup> The calculations corresponding to one iteration are the same as in Table 1.

	SCF-MOM	DO-MOM		
		L-BFGS	L-Powell	L-SR1
Convergence failures	10	0	7	0
Avg no. iterations	26.6	15.1	23.0	12.4
Max no. iterations	121	35	44	16
Min no. iterations	15	9	11	10
Local saddle points	0	2	1	4

for any of the methods. Figure 1 shows the number of iterations needed to converge the singlet states.

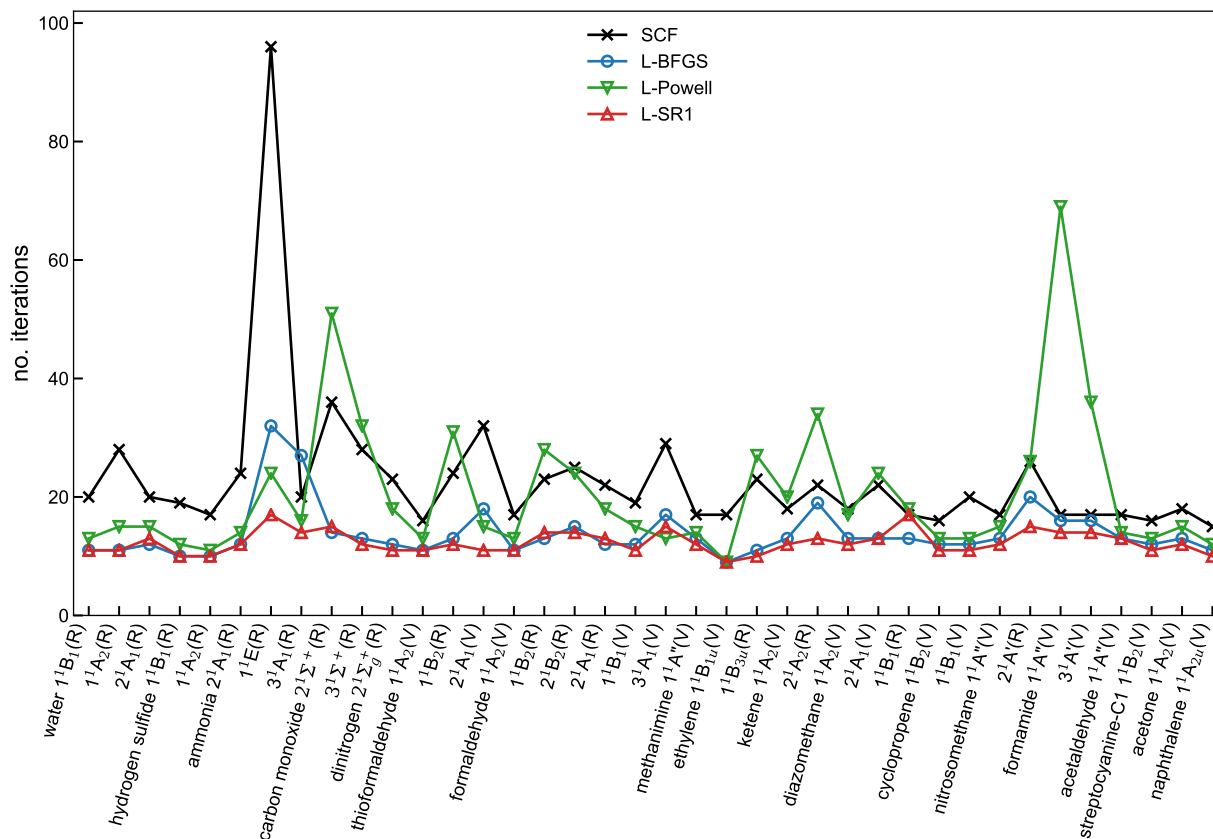


Figure 1: Number of iterations needed to reach convergence of the singlet excited states.

SCF-MOM fails to converge within the maximum number of iterations threshold in about 30% of the cases. All the quasi-Newton algorithms employed within the DO-MOM framework are more robust and show a faster rate of convergence than SCF-MOM. The best performance is obtained with L-SR1, for which all calculations converge, and convergence takes on average about 11 and 14 iterations less than SCF-MOM for singlet and triplet states, respectively. L-BFGS also performs well, being able to converge in all cases except two (the  ${}^1\Delta(\pi \rightarrow \pi^*)$  states of carbon monoxide and dinitrogen). The limited-memory Powell inverse Hessian update in DO-MOM is considerably less efficient than L-SR1 and L-BFGS. L-Powell can have a slow rate of convergence close to a stationary point, which in many cases precludes convergence within the maximum number of allowed iterations. We have tested different combinations of limited-memory inverse Hessian updates by considering some of the cases that are most difficult to converge (see Figure 2). The combination of L-SR1 and L-Powell according to the Bofill approach (see eqs. 20 and 21) is found to have similar performance as L-Powell. This is consistent with the fact that in the Bofill approach  $\phi^k$ , representing the weight of the Powell update, tends to 1 when the optimization approaches a stationary point. We have also tested a combination of L-SR1 and L-BFGS updates using the Bofill factor.<sup>88</sup> This approach does not lead to better convergence compared to L-SR1.

Figure 2 shows the number of iterations needed by DO-MOM with SR1 update to converge the singlet excited states for which the other methods fail. On average these difficult cases require more iterations than the cases presented in Figure 1. Among the states that are difficult to converge are those where excitation occurs from or to a degenerate pair of  $\pi$  orbitals, such as the  $\Pi$  states of hydrogen chloride, carbon monoxide and dinitrogen, while others are high-lying Rydberg states, most of which involve near-degenerate p-type Rydberg orbitals. A particularly challenging situation arises when both the donor and the acceptor orbitals involved in the excitation belong to degenerate pairs, as for the  $\Delta(\pi \rightarrow \pi^*)$  states of carbon monoxide and dinitrogen. In this case, all methods except L-SR1 fail to converge. The other DO-MOM methods exhibit oscillations between different critical points, failing

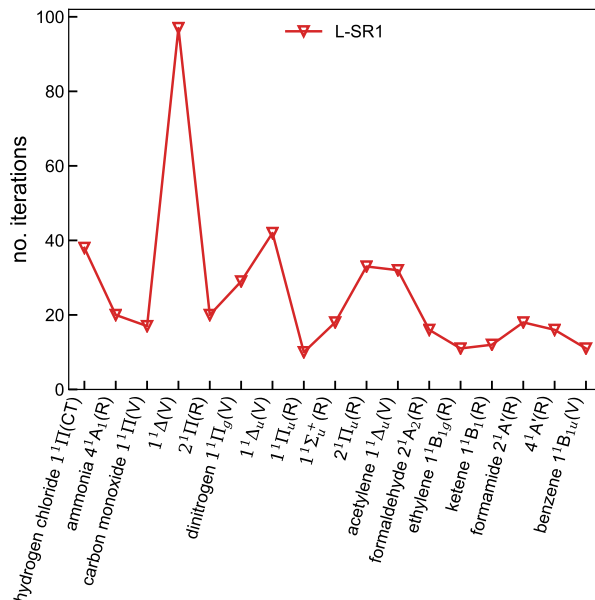


Figure 2: Total number of iterations when DO-MOM with L-SR1 is used to converge the singlet excited states for which SCF-MOM fails.

to converge to the desired solution. The failure of SCF when degenerate orbitals are unequally occupied is discussed in detail below. In about 30% of the calculations that do not converge with SCF-MOM, occupied orbitals can mix with lower-lying empty orbitals of the same symmetry. On the other hand, the L-SR1 method is able to converge all these cases. The properties of DO-MOM when orbitals involved in the excitation are allowed to mix are analyzed in more detail in the following section, where calculations of two totally symmetric excited states of the nitrobenzene molecule are presented.

The SCF convergence problems for states where degenerate orbitals are unequally occupied arise because the electron density represented by a single determinant of KS orbitals obtained at each step is not well defined and this can lead to large changes in the orbitals involved in the excitation from one step to another, and oscillations between different critical points.<sup>40</sup> Several options can be used to help convergence of the SCF: different mixing of the density, alternative DIIS extrapolation techniques,<sup>89</sup> or tuning modifications such as damping, level shifting of the iterations, or electronic smearing.<sup>37</sup> However, DO is able to follow the same solution more consistently without such modifications. It can obtain convergence in

these difficult cases if the chosen quasi-Newton method guarantees sufficiently accurate Hessian updates for the given form of the preconditioner, as shown here. The robustness of the DO approach in calculations involving orbital degeneracies has been previously recognized for ground states of systems with vanishing HOMO-LUMO gap.<sup>40</sup>

For some excited states, a DO method can converge on a solution with higher energy than the solution obtained by SCF or another DO method for the same excited state. For example, the solution obtained for the  $1^1E(n \rightarrow 3p)$  state of ammonia with L-BFGS or L-SR1 DO-MOM lies  $\sim 0.03$  eV higher in energy with respect to the SCF-MOM solution. The occurrence of higher-energy solutions, which we refer to as “local saddle points”, is indicated in Tables 1 and 2. We stress that the multiple solutions that are obtained for a particular case are all saddle points of the same order and correspond to the same excited state. Multiple solutions corresponding to the same excited state are found to differ in the orientation of the highest occupied molecular orbitals (see Figures S2 to S6 in the Supporting Information). Similar to what is observed here for saddle points, the geometric direct minimization method of reference<sup>40</sup> exhibits a tendency to converge on local minima of energy functionals compared to SCF minimizers. Defining the “optimal” approximation to an excited state among multiple variational solutions might not be trivial. Indeed, variational solutions of a nonlinear optimization are in general not orthogonal to one another, and hence higher solutions are not necessarily upper bounds to the exact excited states, but only upper bounds to the ground state.<sup>90</sup> Besides, for many practical applications, such as calculations of PECs or molecular dynamics, one is usually only interested in consistently converging on the same stationary point. For these cases, DO-MOM can be used without modifications. For cases in which the lowest energy saddle point of a given excited state is desired, a possible strategy could be to combine the DO approach with techniques for guiding the convergence towards a global solution, such as the one presented in reference.<sup>91</sup>

Finally, we note that due to the small size of the molecules considered here, the computational effort of SCF-MOM and DO-MOM is comparable, as indicated by similar values of

the elapsed time per iteration. For larger systems, care must be taken that the memory of the quasi-Newton algorithm used within DO-MOM, which here is chosen as  $m = 20$ , does not degrade the computational performance of the method. From test calculations, where we compare the convergence of L-BFGS and L-SR1 with different levels of memory, we find that L-SR1 tends to become less robust with lower memory faster than L-BFGS. Therefore, for large systems, L-BFGS might represent the best compromise between speed of convergence and computational effort among the various limited-memory inverse Hessian update schemes.

### 5.1.2 Nitrobenzene

Figure 3 illustrates the frontier molecular orbitals involved in the electronic transitions that lead to the  ${}^1A_1(n_\pi \rightarrow \pi'^*)$  and  ${}^1A_1(\pi' \rightarrow \pi^*)$  excited states of nitrobenzene. Both states

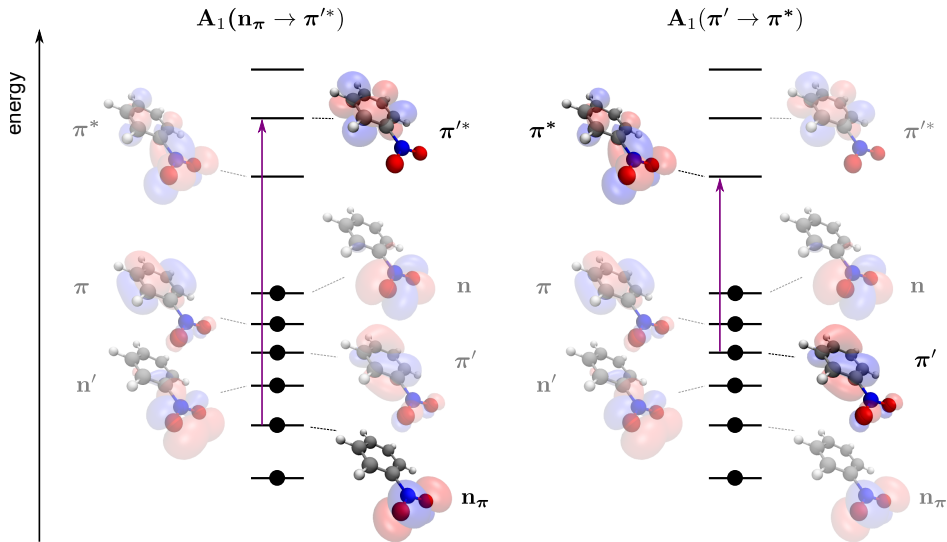


Figure 3: Ground-state frontier molecular orbitals of nitrobenzene and depiction of the electronic transitions involved in the  ${}^1A_1(n_\pi \rightarrow \pi'^*)$  (Left) and  ${}^1A_1(\pi' \rightarrow \pi^*)$  (Right) excited states. The labels of the orbitals are according to the notation from reference.<sup>60</sup> The orbital surfaces are drawn at an isovalue of  $0.1 \text{ \AA}^{-3/2}$ .

have charge-transfer character: in the case of the  ${}^1A_1(n_\pi \rightarrow \pi'^*)$  state, one electron moves from the nitro group to the benzene ring, while in the case of the  ${}^1A_1(\pi' \rightarrow \pi^*)$  state, the direction of the charge transfer is reversed. Figure 3 also schematically illustrates that the

highest occupied orbitals, including the orbital from which excitation occurs, are all closely spaced in energy, covering a range of around 1 eV, despite being localized on different regions of the molecule. Charge transfer from such a subset of closely spaced orbitals is expected to be accompanied by a change of the energy ordering of the occupied orbitals.

Hait *et al.*<sup>21</sup> and Mewes *et al.*<sup>60</sup> have shown that SCF-MOM-based techniques fail to converge to the  ${}^1A_1(n_\pi \rightarrow \pi'^*)$  and  ${}^1A_1(\pi' \rightarrow \pi^*)$  states, respectively. When the overlaps used to find the occupation numbers with the MOM at one step are computed with respect to the orbitals from the previous step, collapse to the ground state occurs; while if the overlaps are computed with respect to the initial set of orbitals, the iterative procedure does not converge. In accord with this, our SCF-MOM calculations exhibit large and rapid oscillations without convergence in 300 iterations. This failure is likely caused by the presence of orbitals energetically close to the  $n_\pi$  and  $\pi'$  orbitals from which excitation occurs, and to rearrangements in the order of the orbital energy levels. DO-MOM, however, is able to converge both of these challenging cases.

Figure 4 shows the convergence of energy and gradient in a DO-MOM calculation of the  ${}^1A_1(n_\pi \rightarrow \pi'^*)$  state using the L-BFGS method, where the preconditioner is updated after the MOM determines a change in the occupation numbers. After 13 steps of the optimization, a change of the character of the occupied orbitals is detected and, as a result, the MOM induces a change in the occupation numbers, which restores the character of the initial guess. Application of the MOM constraints is accompanied by a jump in the energy as can be observed from Figure 4. After that, the energy is converged to  $10^{-6}$  eV in  $\sim 50$  steps. While the approximate Hessian at the initial guess has six negative eigenvalues, the converged solution is a ninth-order saddle point. This is a consequence of a significant rearrangement in the ordering of the orbitals induced by the charge transfer, which stabilizes the orbitals localized on the nitro group, including the hole, and destabilizes the orbitals localized on the benzene ring. When L-BFGS is used, it is essential to apply the MOM constraints and update the preconditioner in order to achieve convergence to the target excited state. This

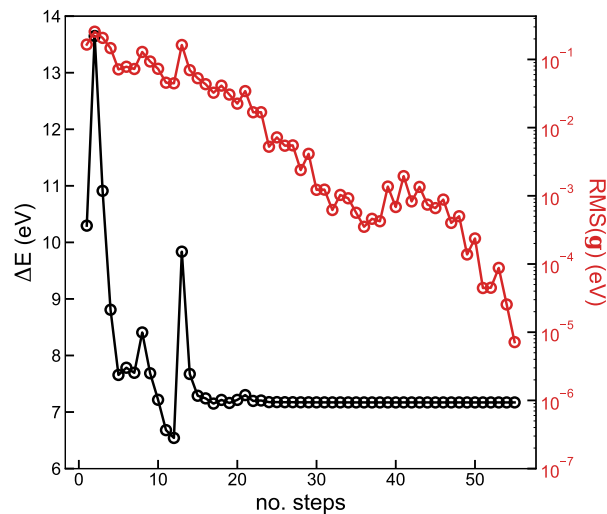


Figure 4: Convergence of excitation energy and root mean square of the gradient in a DO-MOM calculation of the  ${}^1A_1(n_\pi \rightarrow \pi^{*})$  excited state of nitrobenzene using L-BFGS.

is illustrated in Figure 5, which shows a DO calculation with L-BFGS starting from the same initial guess as in Figure 4 but where the MOM is not applied and the preconditioner is not updated. In this case, the hole which has an initial  $n_\pi$  character, acquires during the

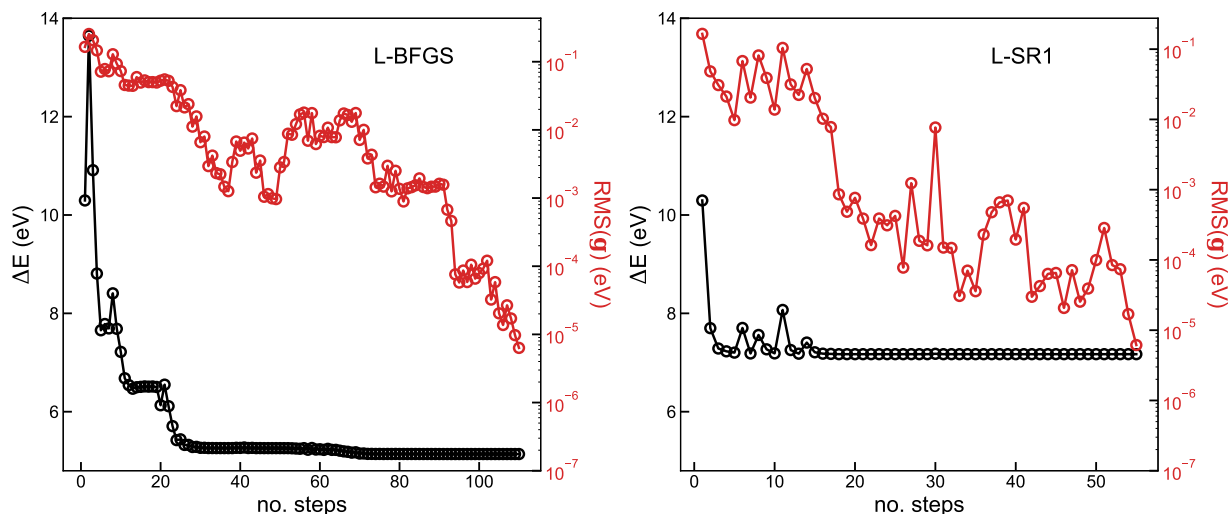


Figure 5: Convergence of excitation energy and root mean square of the gradient in DO calculations using L-BFGS (Left) and L-SR1 (Right) without the MOM and with a preconditioner fixed at the guess for the  ${}^1A_1(n_\pi \rightarrow \pi^{*})$  state of nitrobenzene.

DO the character of the  $\pi$  orbital depicted in Figure 3 (the  $n_\pi$  and  $\pi$  orbitals are allowed to mix because they both belong to the  $A_2$  irreducible representation in the  $C_{2v}$  point group

symmetry), and the calculation eventually collapses to a third-order saddle point. Figure 5 also shows a DO calculation without the MOM and with a fixed preconditioner when the approximate inverse Hessian is updated using L-SR1. Despite an initial approximate Hessian with a lower number of negative eigenvalues compared to the Hessian of the target solution, the DO with L-SR1 is able to converge to the ninth-order saddle point corresponding to the  ${}^1A_1(n_\pi \rightarrow \pi'^*)$  state. This can be explained with the ability of L-SR1 to develop negative eigenvalues, while L-BFGS cannot. The squared gradient minimization method of reference<sup>21</sup> is also able to converge to the  ${}^1A_1(n_\pi \rightarrow \pi'^*)$  state of nitrobenzene. However, due to the need to compute the derivative of the squared norm of the gradient at each step, the minimization involves larger computational effort per iteration than the present DO-MOM calculations.

In the case of the  ${}^1A_1(\pi' \rightarrow \pi^*)$  excited state, the converged solution is found to be a fourth-order saddle point, while the approximate Hessian at the initial guess generated from the ground-state orbitals (see Figure 3) has three negative eigenvalues. As for the  ${}^1A_1(n_\pi \rightarrow \pi'^*)$  state, a DO calculation with L-BFGS can converge to the target solution only if the MOM is used and the preconditioner updated during the optimization.<sup>58</sup> Figure 6 shows the convergence of DO-MOM calculations using L-SR1 with and without preconditioner. It

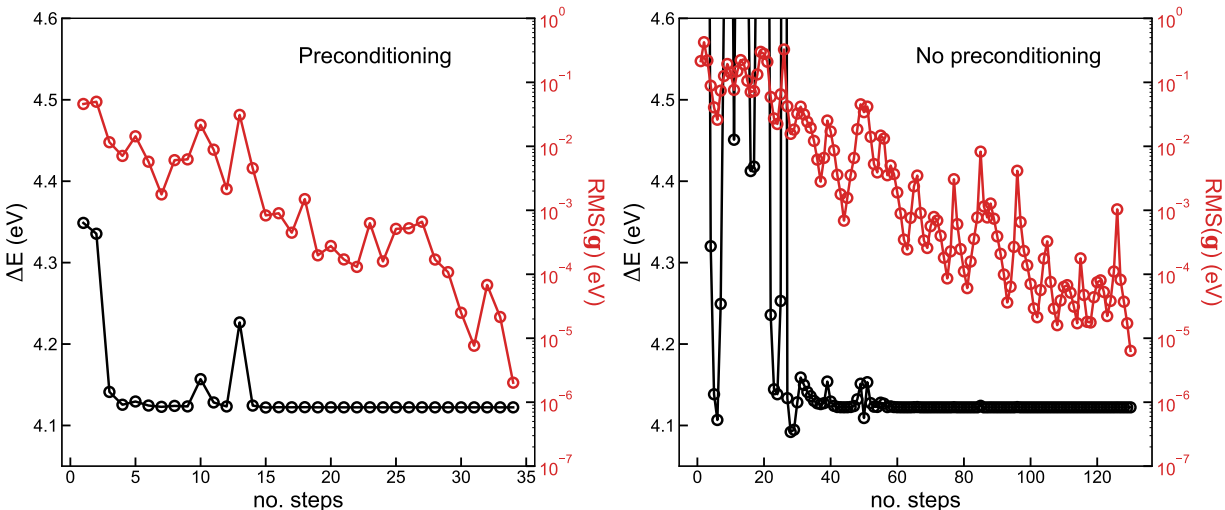


Figure 6: Convergence of excitation energy and root mean square of the gradient in DO-MOM calculations of the  ${}^1A_1(\pi' \rightarrow \pi^*)$  excited state of nitrobenzene using L-SR1 with (Left) and without (Right) preconditioner.

is found that DO-MOM with L-SR1 is able to converge to the  ${}^1A_1(\pi' \rightarrow \pi^*)$  state even without the use of a preconditioner, although large oscillations of the energy are observed at the beginning of the optimization and almost four times as many steps are required to achieve convergence compared to a calculation that uses the preconditioner. These results show that the L-SR1 method developed in the present work is less sensitive to the quality of the preconditioner and is able to build a better approximation to the inverse electronic Hessian when used in optimizations of excited states within DFT compared to a standard implementation of the most used L-BFGS quasi-Newton algorithm.

All calculations presented above use a maximum step length,  $p_{\max}$ , of 0.20, which is the value found optimal in most of the cases. However, a  $p_{\max}$  of 0.25 leads to smaller oscillations at the beginning of the optimization and faster convergence in the case of the DO-MOM calculations with L-SR1 (see Figures S7 and S8 in the Supporting Information). The use of a fixed allowed step length is a limitation of the current implementation. To ensure smooth and monotonic convergence for a broad range of systems, a trust region scheme could be introduced.

### 5.1.3 Potential Energy Curves of Carbon Monoxide

The electron configuration of the ground state of carbon monoxide is  $(1\sigma)^2(1\sigma^*)^2(2\sigma)^2(2\sigma^*)^2(1\pi)^4(3\sigma)^2(1\pi^*)^0(3\sigma^*)^0$ . The lowest singlet excited states arise from  $\sigma \rightarrow \pi^*$  and  $\pi \rightarrow \pi^*$  single-electron excitations. Among the states with these configurations, the  $1^1\Pi(n \rightarrow \pi^*)$  and  $1^1\Delta(\pi \rightarrow \pi^*)$  can be approximated using a single determinant.

KS DFT has several difficulties describing the  $1^1\Pi(n \rightarrow \pi^*)$  and  $1^1\Delta(\pi \rightarrow \pi^*)$  states and their conical intersection. Firstly, the determinant obtained from a single-electron transition between orbitals of the same spin has a broken spin symmetry, since the pure singlet open-shell state is a symmetry-adapted linear combination of two determinants with the same configuration. Secondly, KS DFT neglects the multireference character of the wave

functions arising from mixing of configurations involving the degenerate pairs of  $1\pi$  and  $1\pi^*$  orbitals. Finally, at the conical intersection the  $1\pi$  orbitals become degenerate with the  $3\sigma$  orbital, further increasing the multireference character of the states. The strong static correlation prevents the SCF-MOM method with integer occupation numbers from converging. Convergence can be achieved by smearing the hole and excited electron over the degenerate orbitals. We emphasize that the aim here is not to assess the accuracy of DFT with KS functionals in the description of the excited states, for which highly accurate multireference calculations are available when the molecules are small, but rather to demonstrate the ability of the DO-MOM method to handle a challenging case without *ad hoc* modifications to achieve convergence.

The PECs of the  $1^1\Pi(n \rightarrow \pi^*)$  and  $1^1\Delta(\pi \rightarrow \pi^*)$  states of carbon monoxide around the conical intersection computed using SCF-MOM with Gaussian smearing and DO-MOM are shown in Figure 7 together with the analytical atomic forces for selected points on the  $1^1\Delta(\pi \rightarrow \pi^*)$  curves. For the Gaussian smearing SCF-MOM calculations, far from the conical intersection, the occupation numbers of the  $1\pi$  orbitals are 1 ( $1^1\Pi(n \rightarrow \pi^*)$  state) or 0.5 ( $1^1\Delta(\pi \rightarrow \pi^*)$ ), while the occupation of  $3\sigma$  is either 0 ( $1^1\Pi(n \rightarrow \pi^*)$ ) or 1 ( $1^1\Delta(\pi \rightarrow \pi^*)$ ). Close to the conical intersection, the hole can be smeared over both the  $1\pi$  and  $3\sigma$  orbitals (see Tables S3 and S4 in the Supporting Information). When this happens, the SCF-MOM PECs display some artefacts. The PEC of  $1^1\Pi(n \rightarrow \pi^*)$  shows discontinuities around the three points for which the smearing is largest. The only point of the PEC of  $1^1\Delta(\pi \rightarrow \pi^*)$  for which the hole is smeared over three orbitals coincides approximately with the point of crossing of the two curves ( $R \sim 1.56 \text{ \AA}$ ). The analytical forces computed at this point are not consistent with the slope of the  $1^1\Delta(\pi \rightarrow \pi^*)$  curve.

On the other hand, the curves obtained with DO-MOM PECs and integer occupation numbers do not exhibit discontinuities and the computed atomic forces are consistent with the slopes of the curves. We further note that Gaussian smearing SCF-MOM converges on higher-energy solutions, with the  $1^1\Pi(n \rightarrow \pi^*)$  and  $1^1\Delta(\pi \rightarrow \pi^*)$  PECs computed with DO-

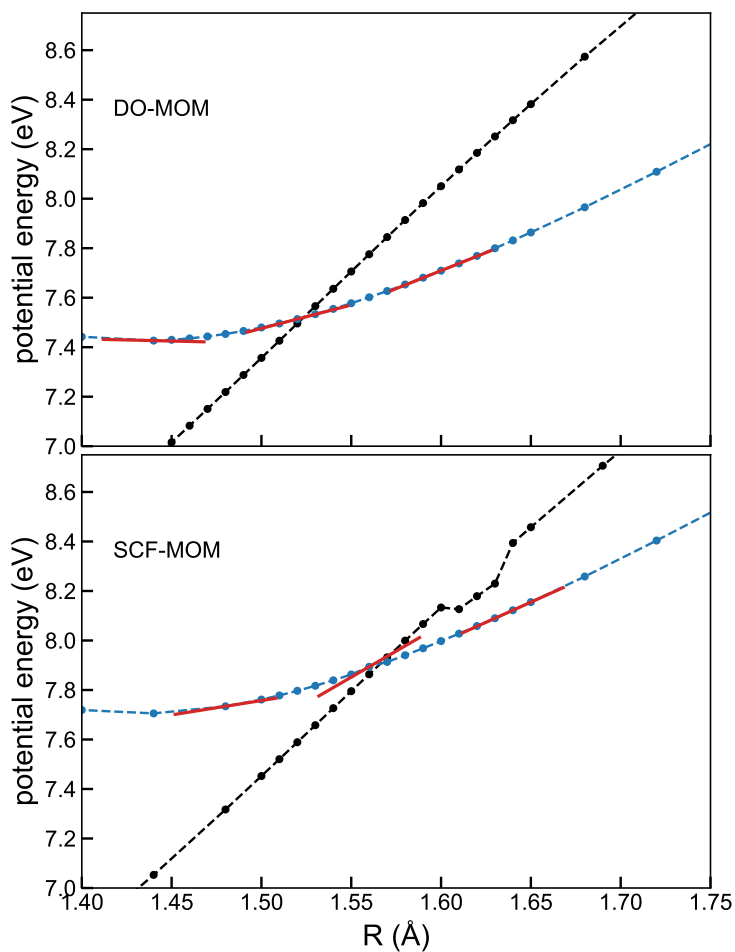


Figure 7: Potential energy curves of the  $1^1\Pi(n \rightarrow \pi^*)$  (black) and  $1^1\Delta(\pi \rightarrow \pi^*)$  (blue) excited states of carbon monoxide computed with the DO-MOM method (top) and a variant of SCF-MOM using Gaussian smearing of the hole and excited electron (bottom). The red lines represent the analytical atomic forces at selected points.

MOM lying respectively  $\sim 0.1$  and  $\sim 0.3$  eV lower in energy with respect to the SCF-MOM PECs. This also affects the relative position of the two conical intersections.

Electronic smearing is often employed together with the SCF method to converge excited-state DFT calculations, especially in molecular dynamics simulations.<sup>22,24,87,92,93</sup> The results presented here show that one needs to carefully check whether artefacts are introduced due

to the smearing. The DO-MOM method can converge energy and forces even in cases of degeneracies without the need of smearing.

## 5.2 Calculations with Self-Interaction Correction

### 5.2.1 Hydrogen Atom

Table 3 reports the energy and eigenvalue of the occupied orbital for the ground state and each of the three lowest excited states of the hydrogen atom computed with PBE and SIC-PBE using DO-MOM, as compared to the experimental values of the ionization energy.

The PBE functional displays a well-known systematic underestimation of the energy of the

Table 3: Total energies (E) and orbital eigenvalues ( $\epsilon$ ) of the ground and the three lowest excited states of the hydrogen atom computed using DO-MOM with PBE and SIC-PBE and experimental values of the ionization (I) energy.<sup>94</sup> The values in parenthesis represent the differences with respect to the experimental energies. All values are in eV.

Electronic state	PBE		SIC-PBE		Exp. <sup>94</sup>
	E	$\epsilon$	E	$\epsilon$	-I
1s	-13.60(0.00)	-7.59(6.01)	-13.60(0.00)	-13.60(0.00)	-13.60
2s	-3.70(-0.30)	-2.23(1.17)	-3.40(0.00)	-3.40(0.00)	-3.40
2p	-3.81(-0.41)	-1.91(1.49)	-3.40(0.00)	-3.40(0.00)	-3.40
3s	-1.73(-0.22)	-1.13(0.38)	-1.50(0.01)	-1.50(0.01)	-1.51

excited states (linear-response TDDFT with PBE predicts no bound Rydberg states for the hydrogen atom).<sup>15</sup> The inability of excited-state DFT with KS semi-local functionals to describe Rydberg series of atoms has been traced back to the fact that the long-range form of the effective potential is incorrect (see, for example, reference<sup>15</sup>).

The SIE of a one-electron system cancels exactly for the SIC-PBE functional. As a result, the SIC-PBE energy values are accurate for the basis set used. Furthermore, for a given state the eigenvalue of the occupied orbital coincides with the total energy and is independent of the occupation number, i.e. for a one-electron system the SIC functional restores the derivative discontinuity that is missing in the approximate functional.<sup>51</sup>

### 5.2.2 Dihydrogen Molecule

Gill *et al.*<sup>23</sup> have recently reported SCF-MOM calculations of the  ${}^1\Sigma_g^+(1\sigma_g^2 \rightarrow 1\sigma_u^2)$  doubly excited state of dihydrogen using xc functionals for several choices of the fraction of exact exchange. Their results show that GGA and hybrid functionals with small fraction of HF exchange severely underestimate the excitation energy because the SIE in the excited state is significantly larger than in the ground state. The DO-MOM PBE calculation of the  ${}^1\Sigma_g^+(1\sigma_g^2 \rightarrow 1\sigma_u^2)$  state is in line with this observation. The PBE excitation energy is 27.25 eV, with a deviation of 1.50 eV from the full configuration interaction (CI) result of reference<sup>23</sup> (28.75 eV). The one-electron SIE calculated according to eq. 9 using the density and the orbitals converged with PBE is  $\sim -1.69$  eV, compared to an SIE of  $\sim -0.10$  eV for the ground state. Therefore, most of the error in the excitation energy comes from an imbalance in the SIEs. If the self-interaction correction is applied non-variationally, the resulting excitation energy is equal to 28.83 eV, which is closer to the full CI result. Further improvement is obtained with the fully variational SIC-PBE calculations giving an excitation energy of 28.79 eV, only 0.04 eV larger than the full CI energy. The remaining error is due to the approximate treatment of correlation and to the use of different basis sets in the DO-MOM SIC-PBE and full CI calculations.

These results illustrate how self-interaction correction in variational DFT calculations of excited states can be an effective route to correct the unbalanced SIE between ground and excited states in calculations based on semi-local functionals.

## 6 Concluding Remarks

DO has long been known to be a robust and computationally competitive alternative to SCF in ground-state calculations.<sup>40,44,45</sup> Calculations using single-determinant excited-state DFT and DO have been limited to minimization of the squared norm of the gradient, while DO of saddle points has been considered to be too difficult, due to the need of a better approxi-

mation to the Hessian and the risk of variational collapse. Here, a DO method is presented that overcomes these challenges by: (1) employing a newly developed limited-memory formulation of quasi-Newton SR1 inverse Hessian update (L-SR1) that is able to build a better approximation to the Hessian for saddle-point searches than the L-BFGS update commonly employed in minimization, and (2) avoiding variational collapse by using MOM constraints. Since only one gradient evaluation is required at each step, the computational cost is the same as for ground-state calculations. We further note that even if DO-MOM has been presented here in the context of excited-state DFT, it can be applied with any other method where the objective is to optimize a set of orthogonal orbitals, provided that the appropriate form of the  $\mathbf{L}$  matrix is used in the expression of the gradient, eq. A.6.

We find that DO-MOM in combination with a localized basis set representation of the orbitals outperforms the conventional SCF-MOM approach both in terms of robustness and speed of convergence for a benchmark set of 89 excited states. The best performance is obtained with the L-SR1 algorithm when using a memory of 20 iterations. Furthermore, tests on challenging charge-transfer excited states of nitrobenzene show that L-SR1 is more robust than L-BFGS for saddle-point optimization, being less dependent on the preconditioner. Therefore, DO-MOM with L-SR1 is a promising method for excited-state calculations of large systems, where diagonalization of the Hamiltonian matrix needed to compute the preconditioner is prohibitive. These tests were limited to valence and Rydberg excited states of small and medium size molecules. In future work these tests will be extended to include larger molecules and long-range charge-transfer states.

DO-MOM is able to converge single-determinant excited states close to conical intersections, which often require fractional occupations in SCF approaches, as demonstrated here for the first two singlet excited states of carbon monoxide. This makes it possible to assess more rigorously the applicability of single-determinant density functional methods for modelling conical intersections as compared to methods that explicitly take into account static correlation effects. Crucially, such benchmarks are currently lacking despite

the fact that excited-state DFT has been proposed in the context of nonadiabatic dynamics simulations<sup>19,22,33</sup>. Formally, the single-determinant approximation is a clear limitation of excited-state DFT. Multiconfigurational effects can be taken into account within, for example, ensemble DFT.<sup>95</sup> Extending the applicability of DO-MOM requires handling the simultaneous optimization of the orbitals and the occupation numbers.<sup>96</sup>

Finally, our implementation of DO-MOM can be used with non-unitary invariant functionals, such as SIC functionals. As pointed out earlier,<sup>11,50</sup> the accuracy of excitation energies obtained with semi-local functionals can be affected by different amounts of SIE in the ground and excited state. The accurate results obtained from the calculations on the lowest doubly excited state of dihydrogen represent a preliminary indication that SIC functionals can help alleviate this issue. However, tests on more complex systems are needed to draw a general conclusion on the performance of SIC functionals. Benchmarks on excited states of molecules, including Rydberg states, are currently ongoing.

## Appendix

### A Exponential Transformation

The spin index is omitted here for simplicity as the exponential transformation does not mix orbitals with different spin quantum number. An initial guess for the optimal orbitals (reference orbitals) is expanded into a linear combination of  $M$  localised basis functions:

$$\phi_p(\mathbf{r}) = \sum_{\mu=1}^M C_{\mu p} \chi_{\mu}(\mathbf{r}) \tag{A.1}$$

The coefficients of this expansion must satisfy the orthonormality constraints:

$$\sum_{\mu\nu} C_{\mu p}^* S_{\mu\nu} C_{\nu q} = \delta_{pq} \tag{A.2}$$

with:

$$S_{\mu\nu} = \int \chi_{\mu}^*(\mathbf{r})\chi_{\nu}(\mathbf{r})d\mathbf{r} \quad (\text{A.3})$$

The optimal orbital coefficients corresponding to an extremum of the energy functional can be found through a unitary transformation of the  $C_{\mu p}$ :

$$O_{\mu k} = \sum_{p=1}^M C_{\mu p} [e^{\boldsymbol{\theta}}]_{pk} \quad (\text{A.4})$$

The  $M \times M$  anti-Hermitian matrix  $\boldsymbol{\theta}$  contains the parameters that describe rotations of the orbitals and is parametrized as:

$$\boldsymbol{\theta} = \begin{pmatrix} \boldsymbol{\theta}_{\text{oo}} & \boldsymbol{\theta}_{\text{ov}} \\ -\boldsymbol{\theta}_{\text{ov}}^{\dagger} & \mathbf{0} \end{pmatrix} \quad (\text{A.5})$$

where the  $N \times N$  block  $\boldsymbol{\theta}_{\text{oo}}$  contains the parameters that describe rotations mixing occupied-occupied (oo) orbitals, while the  $N \times (M - N)$  blocks  $\boldsymbol{\theta}_{\text{ov}}$  mix occupied-virtual (ov) orbitals. The total energy does not depend on rotations among the virtual orbitals and, as a result, the virtual-virtual (vv) block is set to zero. Since  $\boldsymbol{\theta}$  is anti-Hermitian, the total number of free parameters is  $N(2M - N)$ . For KS functionals, the energy is invariant with respect to unitary transformation of equally occupied orbitals and, therefore, the  $\boldsymbol{\theta}_{\text{oo}}$  block can be set to zero without loss of generality.<sup>41</sup> In this case, the number of degrees of freedom is reduced to  $2N(M - N)$  and the matrix exponential can be calculated using the equation given by Hutter *et al.*<sup>41</sup> For SIC functionals,  $\boldsymbol{\theta}_{\text{oo}}$  cannot be set to zero.<sup>54</sup> In this case, the scaling and squaring algorithm of Al-Mohy and Higham<sup>97</sup> as implemented in the SciPy library<sup>98</sup> is used to evaluate the matrix exponential.

In order to carry out the optimization efficiently, using a quasi-Newton method, or any other gradient-based algorithm, the gradient of the energy with respect to the  $\{\theta_{ij}\}$  rotation

parameters is needed:

$$\frac{\partial E}{\partial \theta_{ij}^*} = \frac{2 - \delta_{ij}}{2} \left[ \int_0^1 e^{t\boldsymbol{\theta}} \mathbf{L} e^{-t\boldsymbol{\theta}} dt \right]_{ij} \quad (\text{A.6})$$

where the matrix  $\mathbf{L}$  has elements:

$$L_{lk} = (f_l - f_k)H_{lk} + f_k V_{lk} - f_l V_{kl}^* \quad (\text{A.7})$$

In eq. A.7, the  $H_{lk}$  are the elements of the Hamiltonian matrix in the basis of optimal orbitals:

$$H_{lk} = \sum_{\mu\nu} O_{\mu l}^* H_{\mu\nu} O_{\nu k}, \quad H_{\mu\nu} = \int \chi_{\mu}^*(\mathbf{r}) \mathbf{H}_{\text{KS}} \chi_{\nu}(\mathbf{r}) d\mathbf{r} \quad (\text{A.8})$$

while the  $V_{lk}$  are the elements of orbital-density dependent potentials due to SIC:

$$V_{lk} = \sum_{\mu\nu} O_{\mu l}^* V_{\mu\nu}^k O_{\nu k}, \quad V_{\mu\nu}^k = \int \chi_{\mu}^*(\mathbf{r}) \mathbf{V}_k \chi_{\nu}(\mathbf{r}) d\mathbf{r} \quad (\text{A.9})$$

For KS functionals, the  $V_{lk}$  become zero.

The integral in eq. A.6 can be expanded in a series:

$$\int_0^1 e^{t\boldsymbol{\theta}} \mathbf{L} e^{-t\boldsymbol{\theta}} dt = \mathbf{L} + \frac{1}{2!} [\boldsymbol{\theta}, \mathbf{L}] + \frac{1}{3!} [\boldsymbol{\theta}, [\boldsymbol{\theta}, \mathbf{L}]] + \dots \quad (\text{A.10})$$

When the norm of the matrix  $\boldsymbol{\theta}$  is small ( $\|\boldsymbol{\theta}\| \ll 1$ ), the energy gradient can be estimated accurately using only the first term of this series. During the optimization, the coefficients of the reference orbitals are updated with those of the optimal or canonical orbitals at regular step intervals and, in addition, each time the MOM (see next section) changes the orbital occupations. At every update, the  $\boldsymbol{\theta}$  matrix is reset to zero; therefore, these updates avoid  $\|\boldsymbol{\theta}\|$  becoming too large, thus allowing to use only the first term of the series in eq. A.10 to estimate the gradient.

## B Limited-Memory Powell Update

The Powell inverse Hessian update formula in compact form is:<sup>77</sup>

$$\mathbf{B}_P^{(k+1)} = \mathbf{B}^{(k)} + \mathbf{j}^{(k)} \mathbf{u}^{T(k)} + \mathbf{u}^{(k)} [\mathbf{j}^{T(k)} - (\mathbf{y}^{T(k)} \mathbf{j}^{(k)}) \mathbf{u}^{T(k)}] \quad (\text{B.1})$$

where:

$$\mathbf{u}^{(k)} = \frac{\mathbf{y}^{(k)}}{\mathbf{y}^{T(k)} \mathbf{y}^{(k)}} \quad (\text{B.2})$$

and  $\mathbf{j}^{(k)}$  and  $\mathbf{y}^{(k)}$  are defined as in eqs. 17 and 18, respectively. The product  $\mathbf{B}_P^{(k)} \mathbf{v}^{(k)}$ , where  $\mathbf{v}^{(k)}$  is a vector, can be computed using the following recursive formula:

$$\begin{aligned} \mathbf{B}_P^{(k)} \mathbf{v}^{(k)} = & \mathbf{B}_0^{(k)} \mathbf{v}^{(k)} + \sum_{i=k-m}^{k-1} \mathbf{j}^{(i)} \mathbf{u}^{T(i)} \mathbf{v}^{(k)} \\ & + \sum_{i=k-m}^{k-1} \{ \mathbf{u}^{(i)} [\mathbf{j}^{T(i)} \mathbf{v}^{(k)} - (\mathbf{y}^{T(i)} \mathbf{j}^{(i)}) \mathbf{u}^{T(i)} \mathbf{v}^{(k)}] \} \end{aligned} \quad (\text{B.3})$$

The L-Powell algorithm is obtained by replacing the use of eq. 19 with eq. B.3 in Algorithm 1, which requires storing the vector  $\mathbf{u}^{(k)}$  in addition to  $\mathbf{j}^{(k)}$  at each step (see also Algorithm 1 in reference<sup>58</sup>).

## C Maximum Overlap Method

The MOM method is used to ensure that the character of the occupied optimal orbitals is consistent with the initial guess and to choose the occupation numbers of the canonical orbitals whenever they are needed, e.g. when updating the preconditioner according to eq. 22. The coefficients of the reference orbitals for the MOM, which are used to compute the overlaps with the orbitals at a given step, are chosen as the coefficients  $C_{\mu p}$  of the orbitals

of the initial guess, and are fixed. Accordingly, the overlap matrix at step  $k$  has elements:

$$\Omega_{pl}^{(k)} = \sum_{\nu\mu} C_{p\mu}^* S_{\mu\nu} O_{\nu l}^{(k)} \quad (\text{C.1})$$

where  $S_{\mu\nu}$  is defined according to eq. A.3. The occupied orbitals are chosen as those with the largest projections onto the occupied subspace of the initial guess orbitals:

$$\omega_l^{(k)} = \left[ \sum_{p=1}^N \left( \Omega_{pl}^{(k)} \right)^2 \right]^{\frac{1}{2}} \quad (\text{C.2})$$

If the MOM detects a change of the character of the occupied optimal orbitals, the reference orbitals for the DO are updated. Analogous expressions are used to obtain the occupation numbers of the canonical orbitals when a Hamiltonian diagonalization is performed.

## Acknowledgement

This work was funded by the Icelandic Research Fund (grant number 196070) and the University of Iceland Research Fund. AVI is supported by a doctoral fellowship from the University of Iceland. The authors thank Elvar Ö. Jnsson, Asmus O. Dohn and Myneni Hemanadhan for useful discussions.

## Supporting Information Available

The following files are available free of charge. Basis set convergence tests, data of the convergence tests, additional DO-MOM calculations on nitrobenzene, additional information on the SCF-MOM calculations of the excited-state potential energy curves of carbon monoxide.

## References

- (1) Dreuw, A.; Head-Gordon, M. Single-Reference ab Initio Methods for the Calculation of Excited States of Large Molecules. *Chem. Rev.* **2005**, *105*, 4009–4037.
- (2) Casida, M. E. In *Recent Advances in Density Functional Methods*; Chong, D. P., Ed.; World Scientific, 1995; pp 155–192.
- (3) Runge, E.; Gross, E. K. U. Density-functional theory for time-dependent systems. *Phys. Rev. Lett.* **1984**, *52*, 997–1000.
- (4) Kohn, W.; Sham, L. J. Self-Consistent Equations Including Exchange and Correlation Effects. *Phys. Rev.* **1965**, *140*, 1133–1138.
- (5) Hohenberg, P.; Kohn, W. Inhomogeneous electron gas. *Phys. Rev.* **1964**, *136*, B864.
- (6) Van Meer, R.; Gritsenko, O. V.; Baerends, E. J. Physical meaning of virtual kohn-sham orbitals and orbital energies: An ideal basis for the description of molecular excitations. *J. Chem. Theory Comput.* **2014**, *10*, 4432–4441.
- (7) Levine, B. G.; Ko, C.; Quenneville, J.; Martínez, T. J. Conical intersections and double excitations in time-dependent density functional theory. *Mol. Phys.* **2006**, *104*, 1039–1051.
- (8) Maitra, N. T.; Zhang, F.; Cave, R. J.; Burke, K. Double excitations within time-dependent density functional theory linear response. *J. Chem. Phys.* **2004**, *120*, 5932–5937.
- (9) Tozer, D. J.; Handy, N. C. On the determination of excitation energies using density functional theory. *Phys. Chem. Chem. Phys.* **2000**, *2*, 2117–2121.
- (10) Huix-Rotllant, M.; Nikiforov, A.; Thiel, W.; Filatov, M. In *Density-Functional Methods for Excited States*; Ferré, N., Filatov, M., Huix-Rotllant, M., Eds.; Springer International Publishing: Cham, 2016; pp 445–476.

- (11) Zhao, L.; Neuscamman, E. Density Functional Extension to Excited-State Mean-Field Theory. *J. Chem. Theory Comput.* **2019**, *16*, 164–178.
- (12) Zhekova, H. R.; Seth, M.; Ziegler, T. A perspective on the relative merits of time-dependent and time-independent density functional theory in studies of the electron spectra due to transition metal complexes. An illustration through applications to copper tetrachloride and plastocyanin. *Int. J. Quantum Chem.* **2014**, *114*, 1019–1029.
- (13) Ziegler, T.; Seth, M.; Krykunov, M.; Autschbach, J. A revised electronic Hessian for approximate time-dependent density functional theory. *J. Chem. Phys.* **2008**, *129*, 1–10.
- (14) Seidu, I.; Krykunov, M.; Ziegler, T. Applications of time-dependent and time-independent density functional theory to Rydberg transitions. *J. Phys. Chem. A* **2015**, *119*, 5107–5116.
- (15) Cheng, C. L.; Wu, Q.; Van Voorhis, T. Rydberg energies using excited state density functional theory. *J. Chem. Phys.* **2008**, *129*, 124112.
- (16) Baerends, E. J.; Gritsenko, O. V.; Van Meer, R. The Kohn-Sham gap, the fundamental gap and the optical gap: The physical meaning of occupied and virtual Kohn-Sham orbital energies. *Phys. Chem. Chem. Phys.* **2013**, *15*, 16408–16425.
- (17) Dreuw, A.; Head-Gordon, M. Failure of Time-Dependent Density Functional Theory for Long-Range Charge-Transfer Excited States: The Zinobacteriochlorin-Bacteriochlorin and Bacteriochlorophyll-Spheroidene Complexes. *J. Am. Chem. Soc.* **2004**, *126*, 4007–4016.
- (18) Dreuw, A.; Weisman, J. L.; Head-Gordon, M. Long-range charge-transfer excited states in time-dependent density functional theory require non-local exchange. *J. Chem. Phys.* **2003**, *119*, 2943–2946.

- (19) Mališ, M.; Lubner, S. Trajectory Surface Hopping Nonadiabatic Molecular Dynamics with Kohn-Sham  $\Delta$ SCF for Condensed-Phase Systems. *J. Chem. Theory Comput.* **2020**, *16*, 4071–4086.
- (20) Hait, D.; Head-Gordon, M. Highly Accurate Prediction of Core Spectra of Molecules at Density Functional Theory Cost: Attaining Sub-electronvolt Error from a Restricted Open-Shell Kohn-Sham Approach. *J. Phys. Chem. Lett.* **2020**, *11*, 775–786.
- (21) Hait, D.; Head-Gordon, M. Excited state orbital optimization via minimizing the square of the gradient: General approach and application to singly and doubly excited states via density functional theory. *J. Chem. Theory Comput.* **2020**, *16*, 1699–1710.
- (22) Pradhan, E.; Sato, K.; Akimov, A. V. Non-adiabatic molecular dynamics with  $\Delta$ SCF excited states. *J. Phys.: Condens. Matter* **2018**, *30*, 484002.
- (23) Barca, G. M.; Gilbert, A. T.; Gill, P. M. Simple Models for Difficult Electronic Excitations. *J. Chem. Theory Comput.* **2018**, *14*, 1501–1509.
- (24) Levi, G.; Papai, M.; Henriksen, N. E.; Dohn, A. O.; Møller, K. B. Solution structure and ultrafast vibrational relaxation of the PtPOP complex revealed by  $\Delta$ SCF-QM/MM Direct Dynamics simulations. *J. Phys. Chem. C* **2018**, *122*, 7100–7119.
- (25) Ramos, P.; Pavanello, M. Low-lying excited states by constrained DFT. *J. Chem. Phys.* **2018**, *148*, 144103.
- (26) Liu, J.; Zhang, Y.; Bao, P.; Yi, Y. Evaluating Electronic Couplings for Excited State Charge Transfer Based on Maximum Occupation Method  $\Delta$ SCF Quasi-Adiabatic States. *J. Chem. Theory Comput.* **2017**, *13*, 843–851.
- (27) Park, Y. C.; Senn, F.; Krykunov, M.; Ziegler, T. Self-Consistent Constricted Variational Theory RSCF-CV( $\infty$ )-DFT and Its Restrictions to Obtain a Numerically Stable

- $\Delta$ sCF-DFT-like Method: Theory and Calculations for Triplet States. *J. Chem. Theory Comput.* **2016**, *12*, 5438–5452.
- (28) Park, Y. C.; Krykunov, M.; Ziegler, T. On the relation between adiabatic time dependent density functional theory (TDDFT) and the  $\Delta$ SCF-DFT method. Introducing a numerically stable  $\Delta$ SCF-DFT scheme for local functionals based on constricted variational DFT. *Mol. Phys.* **2015**, *113*, 1636–1647.
- (29) Peng, B.; Van Kuiken, B. E.; Ding, F.; Li, X. A guided self-consistent-field method for excited-state wave function optimization: Applications to ligand-field transitions in transition-metal complexes. *J. Chem. Theory Comput.* **2013**, *9*, 3933–3938.
- (30) Maurer, R. J.; Reuter, K. Excited-state potential-energy surfaces of metal-adsorbed organic molecules from linear expansion  $\Delta$ -self-consistent field density-functional theory ( $\Delta$ -DFT). *J. Chem. Phys.* **2013**, *139*, 014708–014718.
- (31) Himmetoglu, B.; Marchenko, A.; Dabo, I.; Cococcioni, M. Role of electronic localization in the phosphorescence of iridium sensitizing dyes. *J. Chem. Phys.* **2012**, *137*, 154309.
- (32) Kowalczyk, T.; Yost, S. R.; Voorhis, T. V. Assessment of the  $\Delta$ SCF density functional theory approach for electronic excitations in organic dyes. *J. Chem. Phys.* **2011**, *134*, 054128.
- (33) Maurer, R. J.; Reuter, K. Assessing computationally efficient isomerization dynamics:  $\Delta$ SCF density-functional theory study of azobenzene molecular switching. *J. Chem. Phys.* **2011**, *135*, 224303.
- (34) Gilbert, A. T. B.; Besley, N. A.; Gill, P. M. W. Self-consistent field calculations of excited states using the maximum overlap method (MOM). *J. Phys. Chem. A* **2008**, *112*, 13164–71.

- (35) Gavnholt, J.; Olsen, T.; Englund, M.; Schiøtz, J. Delta Self-Consistent Field as a Method to Obtain Potential Energy Surfaces of Excited Molecules on Surfaces. *Phys. Rev. B* **2008**, *78*, 075441.
- (36) Perdew, J. P.; Levy, M. Extrema of the density functional for the energy: Excited states from the ground-state theory. *Phys. Rev. B* **1985**, *31*, 6264–6272.
- (37) Rabuck, A. D.; Scuseria, G. E. Improving self-consistent field convergence by varying occupation numbers. *J. Chem. Phys.* **1999**, *110*, 695–700.
- (38) Huix-Rotllant, M.; Filatov, M.; Gozem, S.; Schapiro, I.; Olivucci, M.; Ferré, N. Assessment of density functional theory for describing the correlation effects on the ground and excited state potential energy surfaces of a retinal chromophore model. *J. Chem. Theory Comput.* **2013**, *9*, 3917–3932.
- (39) Dickson, R. M.; Ziegler, T. A density functional study of the electronic spectrum of permanganate. *Int. J. Quantum Chem.* **1996**, *58*, 681–687.
- (40) Voorhis, T. V.; Head-Gordon, M. A geometric approach to direct minimization. *Mol. Phys.* **2002**, *100*, 1713–1721.
- (41) Hutter, J.; Parrinello, M.; Vogel, S. Exponential transformation of molecular orbitals. *J. Chem. Phys.* **1994**, *101*, 3862–3865.
- (42) Head-Gordon, M.; Pople, J. A. Optimization of wave function and geometry in the finite basis Hartree-Fock method. *J. Phys. Chem.* **1988**, *92*, 3063–3069.
- (43) Douady, J.; Ellinger, Y.; Subra, R.; Levy, B. Exponential transformation of molecular orbitals: A quadratically convergent SCF procedure. I. General formulation and application to closed-shell ground states. *J. Chem. Phys.* **1980**, *72*, 1452–1462.
- (44) Baarman, K.; Vandevondele, J. A comparison of accelerators for direct energy minimization in electronic structure calculations. *J. Chem. Phys.* **2011**, *134*, 244104.

- (45) VandeVondele, J.; Hutter, J. An efficient orbital transformation method for electronic structure calculations. *J. Chem. Phys.* **2003**, *118*, 4365–4369.
- (46) Shea, J. A. R.; Gwin, E.; Neuscamman, E. A Generalized Variational Principle with Applications to Excited State Mean Field Theory. *J. Chem. Theory Comput.* **2020**, *16*, 1526–1540.
- (47) Briggs, E. A.; Besley, N. A. Density Functional Theory Based Analysis of Photoinduced Electron Transfer in a Triazacryptand Based K<sup>+</sup> Sensor. *J. Phys. Chem. A* **2015**, 2902–2907.
- (48) Briggs, E. A.; Besley, N. A.; Robinson, D. QM/MM excited state molecular dynamics and fluorescence spectroscopy of BODIPY. *J. Phys. Chem. A* **2013**, *117*, 2644–2650.
- (49) Levi, G.; Biasin, E.; Dohn, A. O.; Jónsson, H. On the interplay of solvent and conformational effects in simulated excited-state dynamics of a copper phenanthroline photosensitizer. *Phys. Chem. Chem. Phys.* **2019**, *22*, 748–757.
- (50) Gudmundsdóttir, H.; Zhang, Y.; Weber, P. M.; Jónsson, H. Self-interaction corrected density functional calculations of molecular Rydberg states. *J. Chem. Phys.* **2013**, *139*, 194102.
- (51) Perdew, J. P.; Zunger, A. Self-interaction correction to density-functional approximations for many-electron systems. *Phys. Rev. B* **1981**, *23*, 5048–5079.
- (52) Zhang, Y.; Weber, P. M.; Jónsson, H. Self-Interaction Corrected Functional Calculations of a Dipole-Bound Molecular Anion. *J. Phys. Chem. Lett.* **2016**, *7*, 2068–2073.
- (53) Hemanadhan, M.; Shamim, M.; Harbola, M. K. Testing an excited-state energy density functional and the associated potential with the ionization potential theorem. *J. Phys. B: At., Mol. Opt. Phys.* **2014**, *47*, 115005.

- (54) Lehtola, S.; Head-Gordon, M.; Jónsson, H. Complex orbitals, multiple local minima, and symmetry breaking in perded-zunger self-interaction corrected density functional theory calculations. *J. Chem. Theory Comput.* **2016**, *12*, 3195–3207.
- (55) Borghi, G.; Park, C. H.; Nguyen, N. L.; Ferretti, A.; Marzari, N. Variational minimization of orbital-density-dependent functionals. *Phys. Rev. B* **2015**, *91*, 155112.
- (56) Lehtola, S.; Jónsson, H. Variational, Self-Consistent Implementation of the Perdew-Zunger Self-Interaction Correction with Complex Optimal Orbitals. *J. Chem. Theory Comput.* **2014**, *10*, 5324–5337.
- (57) Goedecker, S.; Umrigar, C. J. Critical assessment of the self-interaction-corrected local-density-functional method and its algorithmic implementation. *Phys. Rev. A* **1997**, *55*, 1765.
- (58) Levi, G.; Ivanov, A. V.; Jónsson, H. Variational Calculations of Excited States Via Direct Optimization of Orbitals in DFT. *Faraday Discuss.* **2020**, <https://doi.org/10.1039/D0FD00064G>.
- (59) Nocedal, J.; Wright, S. *Numerical Optimization*; Springer, New York, 2006.
- (60) Mewes, J. M.; Jovanović, V.; Marian, C. M.; Dreuw, A. On the molecular mechanism of non-radiative decay of nitrobenzene and the unforeseen challenges this simple molecule holds for electronic structure theory. *Phys. Chem. Chem. Phys.* **2014**, *16*, 12393–12406.
- (61) Klüpfel, P.; Klüpfel, S.; Tsemekhman, K.; Jónsson, H. Optimization of Functionals of Orthonormal Functions in the Absence of Unitary Invariance. *Lect. Notes Comput. Sci.* **2012**, *7134*, 23.
- (62) Messud, J.; Dinh, P. M.; Reinhard, P.-G.; Suraud, E. On the exact treatment of time-dependent self-interaction correction. *Ann. Phys.* **2009**, *324*, 955.

- (63) Svane, A. Electronic structure of cerium in the self-interaction-corrected local-spin-density approximation. *Phys. Rev. B* **1995**, *53*, 4275–4286.
- (64) Lehtola, S.; Jónsson, H. Correction to Variational, Self-Consistent Implementation of the PerdewZunger Self-Interaction Correction with Complex Optimal Orbitals. *J. Chem. Theory Comput.* **2015**, *11*, 5052–5053.
- (65) Lehtola, S.; Blockhuys, F.; Van Alsenoy, C. An overview of self-consistent field calculations within finite basis sets. *Molecules* **2020**, *25*, 1–23.
- (66) Olsen, R. A.; Kroes, G. J.; Henkelman, G.; Arnaldsson, A.; Jónsson, H. Comparison of methods for finding saddle points without knowledge of the final states. *J. Chem. Phys.* **2004**, *121*, 9776–9792.
- (67) Bofill, J. M. Updated Hessian matrix and the restricted step method for locating transition structures. *J. Comput. Chem.* **1994**, *15*, 1–11.
- (68) Culot, P.; Dive, G.; Nguyen, V. H.; Ghuysen, J. M. A quasi-Newton algorithm for first-order saddle-point location. *Theor. Chim. Acta* **1992**, *82*, 189–205.
- (69) Baker, J. An algorithm for the location of transition states. *J. Comput. Chem.* **1986**, *7*, 385–395.
- (70) Simons, J.; Jørgensen, P.; Taylor, H.; Ozment, J. Walking on potential energy surfaces. *J. Phys. Chem.* **1983**, *87*, 2745–2753.
- (71) Cerjan, C. J.; Miller, W. H. On finding transition states. *J. Chem. Phys.* **1981**, *75*, 2800–2806.
- (72) Enkovaara, J.; Rostgaard, C.; Mortensen, J. J.; Chen, J.; Dulak, M.; Ferrighi, L.; Gavnholt, J.; Glinsvad, C.; Haikola, V.; Hansen, H. A.; Kristoffersen, H. H.; Kuisma, M.; Larsen, A. H.; Lehtovaara, L.; Ljungberg, M.; Lopez-Acevedo, O.; Moses, P. G.; Ojanen, J.; Olsen, T.; Petzold, V.; Romero, N. A.; Stausholm-Møller, J.; Strange, M.;

- Tritsaris, G. A.; Vanin, M.; Walter, M.; Hammer, B.; Häkkinen, H.; Madsen, G. K. H.; Nieminen, R. M.; Nørskov, J. K.; Puska, M.; Rantala, T. T.; Schiøtz, J.; Thygesen, K. S.; Jacobsen, K. W. Electronic structure calculations with GPAW: a real-space implementation of the projector augmented-wave method. *J. Phys.: Condens. Matter* **2010**, *22*, 253202.
- (73) Larsen, A. H.; Vanin, M.; Mortensen, J. J.; Thygesen, K. S.; Jacobsen, K. W. Localized atomic basis set in the projector augmented wave method. *Phys. Rev. B* **2009**, *80*, 195112.
- (74) Mortensen, J.; Hansen, L.; Jacobsen, K. W. Real-space grid implementation of the projector augmented wave method. *Phys. Rev. B* **2005**, *71*, 035109.
- (75) Bofill, J. M.; Comajuan, M. Analysis of the updated Hessian matrices for locating transition structures. *J. Comput. Chem.* **1995**, *16*, 1326–1338.
- (76) Anglada, J. M.; Besalú, E.; Bofill, J. M.; Rubio, J. Another way to implement the Powell formula for updating Hessian matrices related to transition structures. *J. Math. Chem.* **1999**, *25*, 85–92.
- (77) Sun, W.; Yuan, Y.-X. *Optimization Theory and Methods*; Springer, Boston, 2006.
- (78) Blöchl, P. E. Projector augmented-wave method. *Phys. Rev. B* **1994**, *50*, 17953.
- (79) Pulay, P. Convergence acceleration of iterative sequences. the case of scf iteration. *Chem. Phys. Lett.* **1980**, *73*, 393–398.
- (80) Perdew, J. P.; Burke, K.; Ernzerhof, M. Generalized gradient approximation made simple. *Phys. Rev. Lett.* **1996**, *77*, 3865.
- (81) Loos, P. F.; Scemama, A.; Blondel, A.; Garniron, Y.; Caffarel, M.; Jacquemin, D. A Mountaineering Strategy to Excited States: Highly Accurate Reference Energies and Benchmarks. *J. Chem. Theory Comput.* **2018**, *14*, 4360–4379.

- (82) Schreiber, M.; Silva-Junior, M. R.; Sauer, S. P.; Thiel, W. Benchmarks for electronically excited states: CASPT2, CC2, CCSD, and CC3. *J. Chem. Phys.* **2008**, *128*, 134110.
- (83) Woon, D. E.; Dunning, T. H. Gaussian basis sets for use in correlated molecular calculations. III. The atoms aluminum through argon. *J. Chem. Phys.* **1993**, *98*, 1358–1371.
- (84) Kendall, R. A.; Dunning, T. H.; Harrison, R. J. Electron affinities of the first-row atoms revisited. Systematic basis sets and wave functions. *J. Chem. Phys.* **1992**, *96*, 6796–6806.
- (85) Dunning, T. H. Gaussian basis sets for use in correlated molecular calculations. I. The atoms boron through neon and hydrogen. *J. Chem. Phys.* **1989**, *90*, 1007–1023.
- (86) Weigend, F.; Ahlrichs, R. Balanced basis sets of split valence, triple zeta valence and quadruple zeta valence quality for H to Rn: Design and assessment of accuracy. *Phys. Chem. Chem. Phys.* **2005**, *7*, 3297–3305.
- (87) Abedi, M.; Levi, G.; Zederkof, D. B.; Henriksen, N. E.; Ppai, M.; Mller, K. B. Excited-state solvation structure of transition metal complexes from molecular dynamics simulations and assessment of partial atomic charge methods. *Phys. Chem. Chem. Phys.* **2019**, *21*, 4082–4095.
- (88) Hratchian, H. P.; Schlegel, H. B. In *Theory and Applications of Computational Chemistry*; Dykstra, C. E., Frenking, G., Kim, K. S., Scuseria, G. E., Eds.; Elsevier: Amsterdam, 2005; pp 195 – 249.
- (89) Garza, A. J.; Scuseria, G. E. Comparison of self-consistent field convergence acceleration techniques. *J. Chem. Phys.* **2012**, *137*, 54110.
- (90) Helgaker, T.; Jrgensen, P.; Olsen, J. *Molecular Electronic Structure Theory*; John Wiley & Sons, Ltd, 2014; Chapter 4, pp 107–141.

- (91) Vaucher, A. C.; Reiher, M. Steering Orbital Optimization out of Local Minima and Saddle Points Toward Lower Energy. *J. Chem. Theory Comput.* **2017**, *13*, 1219–1228.
- (92) Dohn, A. O.; Kjær, K. S.; Harlang, T. B.; Canton, S. E.; Nielsen, M. M.; Møller, K. B. Electron Transfer and Solvent-Mediated Electronic Localization in Molecular Photocatalysis. *Inorg. Chem.* **2016**, *55*, 10637–10644.
- (93) Dohn, A. O.; Jónsson, E. O.; Kjær, K. S.; B. van Driel, T.; Nielsen, M. M.; Jacobsen, K. W.; Henriksen, N. E.; Møller, K. B. Direct Dynamics Studies of a Binuclear Metal Complex in Solution: The Interplay Between Vibrational Relaxation, Coherence, and Solvent Effects. *J. Phys. Chem. Lett.* **2014**, *5*, 2414–2418.
- (94) Kramida, A.; Yu. Ralchenko,; Reader, J.; NIST ASD Team, NIST Atomic Spectra Database (ver. 5.7.1), [Online]. Available: <https://physics.nist.gov/asd> [2020, April 23]. National Institute of Standards and Technology, Gaithersburg, MD., 2019.
- (95) Theophilou, A. K. The energy density functional formalism for excited states. *J. Phys. C: Solid State Phys.* **1979**, *12*, 5419–5430.
- (96) Nygaard, C. R.; Olsen, J. A second-order unconstrained optimization method for canonical-ensemble density-functional methods. *J. Chem. Phys.* **2013**, *138*, 1–13.
- (97) Al-Mohy, A.; Higham, N. A new scaling and squaring algorithm for the matrix exponential. *SIAM J. Matrix Anal. Appl.* **2009**, *31*, 970–989.
- (98) Virtanen, P.; Gommers, R.; Oliphant, T. E.; Haberland, M.; Reddy, T.; Cournapeau, D.; Burovski, E.; Peterson, P.; Weckesser, W.; Bright, J.; van der Walt, S. J.; Brett, M.; Wilson, J.; Jarrod Millman, K.; Mayorov, N.; Nelson, A. R. J.; Jones, E.; Kern, R.; Larson, E.; Carey, C.; Polat, İ.; Feng, Y.; Moore, E. W.; VanderPlas, J.; Laxalde, D.; Perktold, J.; Cimrman, R.; Henriksen, I.; Quintero, E. A.; Harris, C. R.; Archibald, A. M.; Ribeiro, A. H.; Pedregosa, F.; van Mulbregt, P.; SciPy 1.0 Contrib-

utors, SciPy 1.0: Fundamental Algorithms for Scientific Computing in Python. *Nat. Methods* **2020**, *17*, 261–272.

# TOC Graphic

